# SANDIA REPORT

SAND2003-8800
Unlimited Release
Printed December 2003

# LIGA Microsystems Aging: Evaluation and Mitigation

N. Y. C. Yang, C. San Marchi, C. Cadden

Prepared by
Sandia National Laboratories
Albuquerque, New Mexico 87185 and Livermore, California 94550

Sandia is a multiprogram laboratory operated by Sandia Corporation,
a Lockheed Martin Company, for the United States Department of Energy's
National Nuclear Security Administration under Contract DE-AC04-94AL85000.



Sandia National Laboratories

Issued by Sandia National Laboratories, operated for the United States Department of Energy by Sandia Corporation.



Available to DOE and DOE contractors from
U.S. Department of Energy
Office of Scientific and Technical Information
P.O. Box 62
Oak Ridge, TN 37831

Telephone: (865)576-8401
Facsimile: (865)576-5728
E-Mail: reports@adonis.osti.gov
Online ordering: http://www.osti.gov/bridge

Available to the public from
U.S. Department of Commerce
National Technical Information Service
5285 Port Royal Rd
Springfield, VA 22161

Telephone: (800)553-6847
Facsimile: (703)605-6900
E-Mail: orders@ntis.fedworld.gov
Online order: http://www.ntis.gov/help/ordermethods.asp?loc=7-4-0#online

SAND 2003-8800
Unlimited Release
Printed December 2003

# LIGA Microsystems Aging: Evaluation and Mitigation

Nancy Y.C. Yang
Materials Chemistry

Chris San Marchi and Chuck Cadden
Engineered Materials Department
Sandia National Laboratories
P. O. Box 969
Livermore, CA

## Abstract

The deployment of LIGA structures in DP applications requires a thorough understanding of potential long term physical and chemical changes that may occur during service. While these components are generally fabricated from simple metallic systems such as copper, nickel and nickel alloys, the electroplating process used to form them creates microstructural features which differ from those found in conventional (e.g. ingot metallurgy) processing of such materials. Physical changes in non-equilibrium microstructures may occur due to long term exposure to temperatures sufficient to permit atomic and vacancy mobility. Chemical changes, particularly at the surfaces of LIGA parts, may occur in the presence of gaseous chemical species (e.g. water vapor, HE off-gassing compounds) and contact with other metallic structures.

In this study, we have characterized the baseline microstructure of several nickel-based materials that are used to fabricate LIGA structures. Solute content and distribution was found to have a major effect on the electroplated microstructures. Microstructural features were correlated to measurements of hardness and tensile strength. Dormancy testing was conducted on one of the baseline compositions, nickel-sulfamate. Groups of specimens were exposed to controlled thermal cycles; subsequent examinations compared properties of "aged" specimens to the baseline conditions. Results of our testing indicate that exposure to ambient temperatures (-54°C to 71°C) do not result in microstructural changes that might be expected to significantly effect mechanical performance. Additionally, no localized changes in surface appearance were found as a result of contact between electroplated parts.

This page intentionally left blank

# Contents



List of Figures

List of Tables

# Introduction

The deployment of LIGA structures in DP applications requires a thorough understanding of potential long term physical and chemical changes that may occur during service. While these components are generally fabricated from simple metallic systems such as copper, nickel and nickel alloys, the electroplating process used to form them creates microstructural features which differ from those found in conventional (e.g. ingot metallurgy) processing of such materials. Physical changes in non-equilibrium microstructures may occur due to long term exposure to temperatures sufficient to permit atomic and vacancy mobility. Chemical changes, particularly at the surfaces of LIGA parts, may occur in the presence of gaseous chemical species (e.g. water vapor, HE off-gassing compounds) and contact with other metallic structures.

This report documents the results of two related efforts; results are presented accordingly. The first section summarizes efforts to characterize the baseline properties of LIGA electrodeposits formed in several material systems. Microstructure and hardness of various nickel-based compositions (Ni-sulfamate, Ni-saccharin, Ni-Co and Ni-Mn) are presented. The effect of thermal exposure upon microstructural stability is also documented. In the second part of this report, dormancy experiments are described and results presented. These experiments were conducted using only one material (nickel plated from a nickel sulfamate bath). Specimens were evaluated in the as-manufactured condition; evaluations were repeated after thermal cycling in a controlled environment. Mechanical strength, hardness and microstructure are compared to baseline standards.

# Characterization of the Baseline Prototype LIGA Electrodeposits

## Introduction

In this report, we will describe: (A) materials fabrication including composition, sample design and electrodeposition process; (B) metallurgical characterization; (C) summary and discussion; and (D) conclusions. A major emphasis is placed on the metallurgical characterization section. In this section, we will present: (i) experimental procedure; (ii) experimental data and results of metallurgy including microstructure, hardness and texture; (iii) thermal stability of each baseline material; and (iv) surface finishing of LIGA micro components.

## Test Materials

The test pattern designs for the samples used in this study are shown in Figure 1. Thickness of the deposits ranged from 200 to 400um. They were electroplated in lithographically defined PMMA molds and released from 3-inch metalized wafers. Linear pattern, Figure 1f, is about 400 um thick, overplated and unreleased. The pattern contained lines of multiple aspect ratios (thickness/width). Figure 1g is a mold-free deposit plated on a 1-inch rotating Cu disk which often served as a precursor for scoping LIGA electrodeposition parameters.

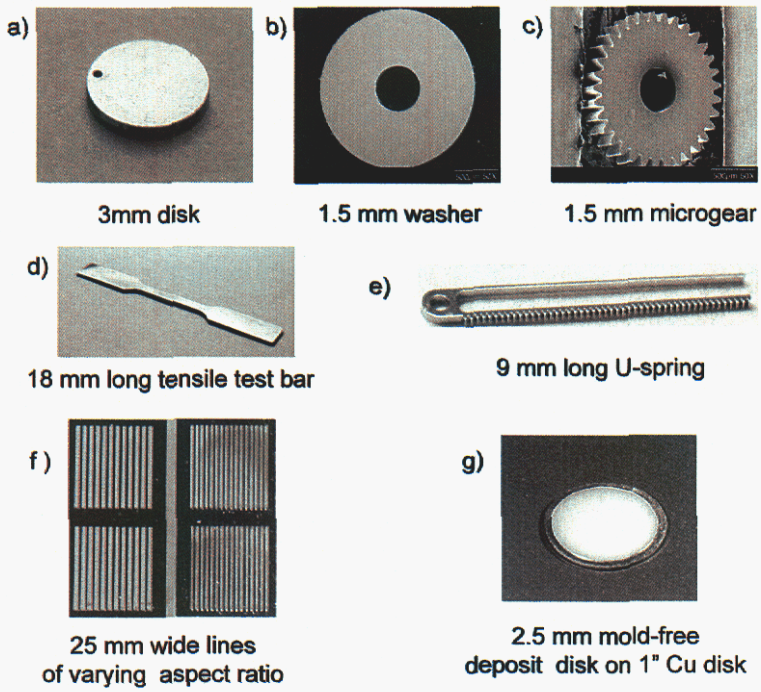


Figure 1. Test pattern designs

Four baseline LIGA materials were examined; Ni-sulfamate, Ni-Mn (~0.5wt %), Ni-Co (~30wt %), and Ni-saccharin (stress-relief additive). All four materials were electroplated in the sulfamate-based electrolyte bath (see compositions below) at 50C, pH 3.5, and a current density of 15mA/cm2.

Composition of electrolyte

497 g/L Ni sulfamate salt, 45 g/L boric acid,
0.2 g/L sodium lauryl sulfate (SLS). "burnt in"15 $mA/cm^2$

- For Ni-saccharin, 2g/L saccharin salt is added
- For Ni-Mn, Mn-chloride (~5g/L Mn in the bath) is added
- For Ni-Co, Co-sulfamate (5 to 50g/L Co in the bath) is added

## Metallurgical characterization

### (i) Experimental procedures

Metallurgical characteristics (microstructure, alloy composition and its distribution, hardness and texture) were examined on the longitudinal cross sections (see Figure 2). The longitudinal section allows us to investigate metallurgical variations through thickness, along the plating direction (PD).

- *Sample preparation*

Transverse and longitudinal cross sections were sliced from the deposit with or without substrates as shown in the following schematic. The cross-sectional surfaces were ground and polished using standard metallographic techniques. Samples were sequentially ground with 200, 400, 600 grit SiC papers followed by 6, 2, and 1 μm $Al_2O_3$ slurries. The surface at the end of the process was a scratch-free, mirror finish. In this study, almost all the examination was conducted on the longitudinal cross section so that composition and property variations through the thickness of the electrodeposits could be evaluated. A few transverse thin film sections, <200nm thick, were electropolished (5% perchloric acid) for the transmission electron microscopy study of atomistic- related microstructure .

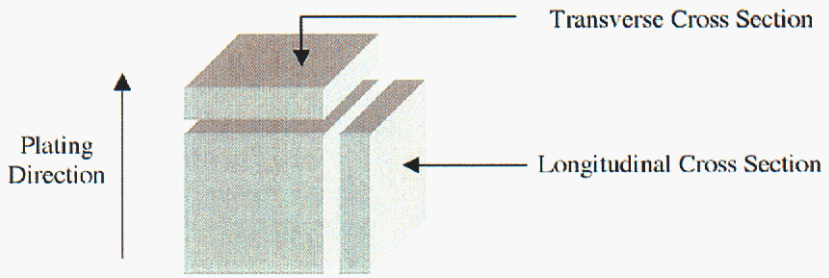


Figure 2: Schematic of the sample cross section.

- *Chemical composition measurements*

Composition profiles of the alloying elements Ni, Co and Mn were measured using quantitative electron microprobe with wavelength disperse X-ray spectroscopy analyses (EMPA/WDS). The analyses are conducted on the as-polished longitudinal cross section of the electrodeposits using a fully automated JEOL-8200 Superprobe employing five spectrometers.

- *Microstructure examination*

Grain morphology and size are estimated using scanning electron microscopy-backscattered electron images (SEM/BEI). These SEM/BEI images were generated using a JEOL Model 840 microscope equipped with angular backscattered electron detector.

For samples with submicron size grains, <1.0 um, the grain structure was imaged in a dual-beam FIB (focused ion beam) instrument manufactured by FEI Company, Model Strata DB235. The image contrasts are focus ion beam induced secondary electron images. In addition, a Philips CM30 transmission electron microscope / bright field /dark field (TEM/BF/DF) was used to examine atomistic microstructure such as twins, dislocations and submicrometer-size lattice defects.

- *Grain Size measurements*

Grain morphology in the as-plated LIGA electrodeposits was generally columnar or acicular with an aspect ratio greater than 5 and a width on the order of a micrometer. The grain size in this study is defined as the average width of the columnar features. The features include regular high angle grains and twins, which often are indistinguishable in SEM –BEI images.

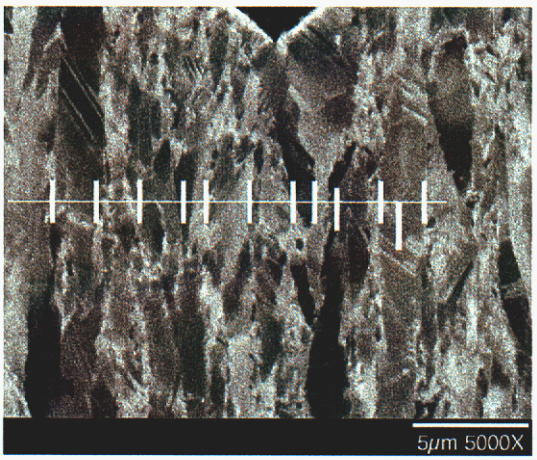


Intergranular spacing (grain width) = a X (b/c)/d = 5 X (65/11) /18 = 1.6um

a: calibrated length scale
b: total length for intercepts
c: number of intercepts
d: Length of calibrated scale bar

Figure 3. Intercept method used for calculation of grain size.

The technique used for grain size measurement is an intercept method utilizing SEM-BEI and/or FIB-SEI images as illustrated in Figure 3.

- *Microhardness measurements*

Microhardness measurements for the current electrodeposits were carried out using an automated Leco M-400 indentation system with Vicker's diamond indenter. A typical diamond indentation is shown in Figure 4. All measurements were conducted on longitudinal cross sections. Hardness of the deposit was typically obtained from measurements taken at five locations along the thickness in the plating direction (1.0mm off the released surface, t/4, t/2, 3t/4, and 1.0mm off the lapped surface) to evaluate the hardness gradient through the thickness as shown in the Figure 4.

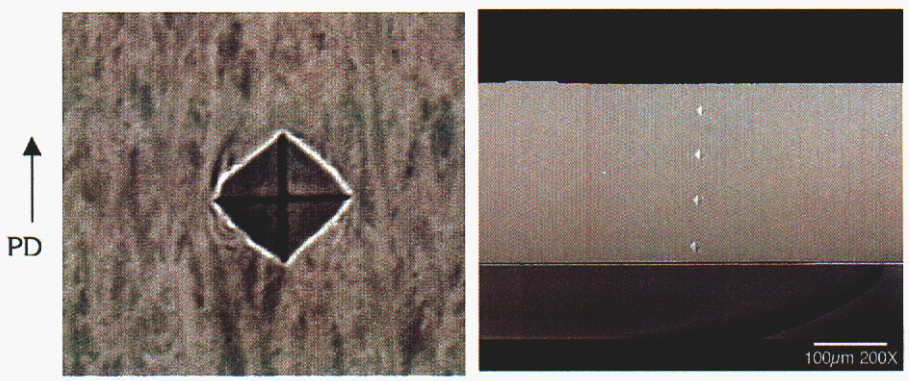


Figure 4. Hardness indentation (left) and through-thickness location of indentations (right).

Hardness is a measure of resistance to penetration and is derived from the following formula:

$VHN = 1.8544 \times L / d^2$

L: Load (kg); typical load used for LIGA deposits is 25g
d: mean value of indentation diagonals (mm)

- *Texture*

Texture orientations along the plating direction were obtained using electron backscattered diffraction patterns (EBSP) by SEM along with X-ray diffraction (XRD). The two techniques are complementary. XRD is a bulk analysis measurement for features larger than 100 μm, and EBSP is a microanalysis measurement for individual features larger than 1.0 μm.

- *Surface finishing*

Examination of surface finish was conducted on the test patterns which were lapped and released from the wafers using SEM/SEI. All surfaces were examined: the lapped and

released surfaces as well as the sidewalls. Optical microscopy was used to supplement the SEM/SEI information, particularly with respect to surface topography. Sidewall surfaces of the PMMA mold were also examined to determine how those surfaces are influenced by the lithography process.

**(ii) Metallurgical data and results**

(a) Ni-sulfamate

This analysis was conducted on five low aspect ratio test patterns; 3-mm disks, tensile test bars, washers, microgears and U-springs. These samples were plated in two different plating tanks, Tank 13 and Tank 14 (referred as Lot 13 and Lot 14). Results indicate that metallurgical properties of deposits from the two lots were very different. However, among the deposits from the same lot, metallurgical properties were quite consistent regardless of the pattern design (see Table I).

**Table I: Summaries of the metallurgical properties of Ni-sulfamate**

| | | Grain structure | | Hardness (VHN) | texture | Impurity (ppm) |
|---|---|---|---|---|---|---|
| | | Morphology | grain size (um) | | | |
| Lot 14 (SEM#13) | 1-inch disk | Columnar | 2-5um | 180 | [100] | Total of Co, Cu, Mo, Zn <350 ppm |
| | Washer | Columnar | | 200 | [100] | |
| | Microgear | Columnar | | 210 | [100] | |
| | U-spring | Columnar | | 180 | [100] | |
| | Tensile bar | Columnar | | 218 | [100] | |
| Lot 13 (SEM #14) | 1-inch disk | Columnar | 0.3-0.6um | N/A | [110] | Total of Co, Cu, Mo, Zn >800 ppm |
| | Washer | Columnar | | 340 | [110] | |
| | Microgear | Columnar | | 330 | [110] | |
| | U-spring | Columnar | | 320 | [110] | |
| | Tensile bar | Columnar | | N/A | [110] | |

Microstructure

SEM/BEI images show that Ni-sulfamate microstructure for both Lot 13 and Lot 14 in general is quite uniform through the thickness (Figure 5a,c). FIB images show that grains typically were columnar with the long axis parallel to the plating direction (PD) (Fig. 5b,d). The columnar grain width (perpendicular to the PD) was about 1-5 um depending on the lot. The grain size of the deposits from Lot 13 was uncharacteristically small. The coarse microstructure of the deposits from Lot 14 is

more typical for Ni-sulfamate deposits (Ref. 1-3). TEM/BF/DF images of the plan view of deposits from lot 13 show few widely spaced twins (light band in the DF image) in the otherwise clean matrix (Fig.5e,f).

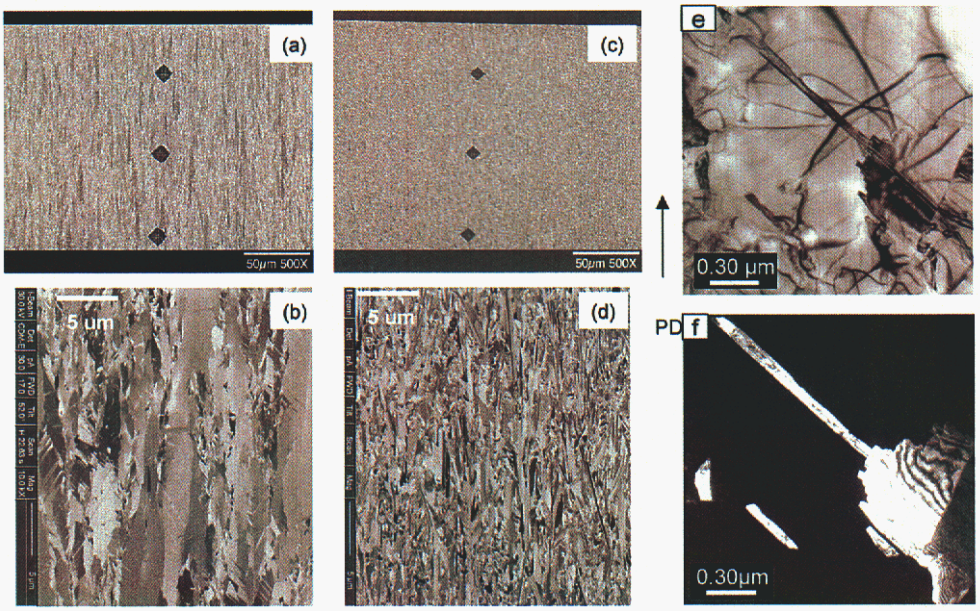


Figure 5. SEM/BEI, FIB and TEM/BF/DF images show typical grain structure of Ni-sulfamte deposits. (a-b) BEI and FIB for Lot 14, (c-d) BEI and FIB for Lot 13, (e-f) TEM/BF/DF image pair show twins (light bands) for Lot 13. The dark diamonds in the BEI (a) and (c) images are artifacts from the hardness indentations.

Vickers hardness

The Vickers hardness measured from the five points through the thickness was relatively uniform. Average VHN for the deposits from the Lot 13 and Lot 14 are distinctly different however, measuring ~ 330 and ~200 VHN, respectively (See Table I).

Texture

EBSP (Electron Backscattered Patterns) show that the Ni-sulfamate deposits are anisotropic and possess texture of [100] and [110] for the Lot 14 and 13, respectively (Fig. 6). [100] texture of Ni-sulfamate deposits was also observed by others (Ref. 4-5).

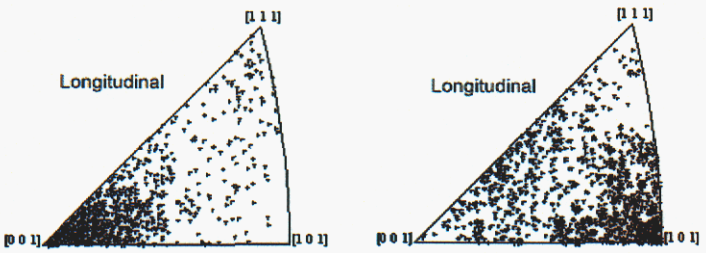


Texture for Lot 14 Texture for Lot 13

Figure 6. Typical inverse pole figures for EBSP showing texture in Ni-sulfamate material from (left) Lot 14, (right) Lot 13

Impurities concentration

Impurity concentrations were measured by glow discharged mass spectroscopy (GDMS). The results shows that most noticeable impurities in the current Ni-sulfamate deposits were Cu, Zn, Co and Mo. The total impurity concentration of these four elements in the deposits from Lot 14 and Lot 13 were ~330ppm and ~ 800ppm, respectively.

## (b) Ni-Mn (~0.5wt %)

Based on the Ni-Mn phase diagram (Ref. 6), Ni and Mn form a solid solution up to 9-10 wt% Mn. At concentrations greater than 0.5wt% Mn, the plating stress is too high to be practical for plating complex high aspect ratio microcomponents. The Ni -0.5wt % Mn composition was chosen taking into account plating stress considerations (Ref. 7).

Alloy composition and its uniformity

Examination of Ni-Mn structures was restricted to specimens with the tensile bar geometry. Compositional analyses measured by EMPA/WDS showed that among the many deposits examined, the average composition could vary 20-40 % from the nominal 0.5 wt% of the alloy. In addition, these analyses frequently indicated a through-thickness manganese gradient along the plating direction (PD) (Fig. 7b). The gradient is especially pronounced for alloys with relatively low Mn, < 0.3wt %. The magnitude of this Mn variation through the thickness can be 20-50% of the average concentration.

Microstructure

SEM/BEI images showed that Ni-Mn microstructural features are macroscopically uniform through the thickness and grains are submicrometer in size (Fig. 8a). Microstructural features are extremely fine (<<1.0um) and the grain morphology of the individual grains is too small to be revealed by the SEM/BEI images. For these submicrometer grains, FIB imaging is required to examine the grain structure,

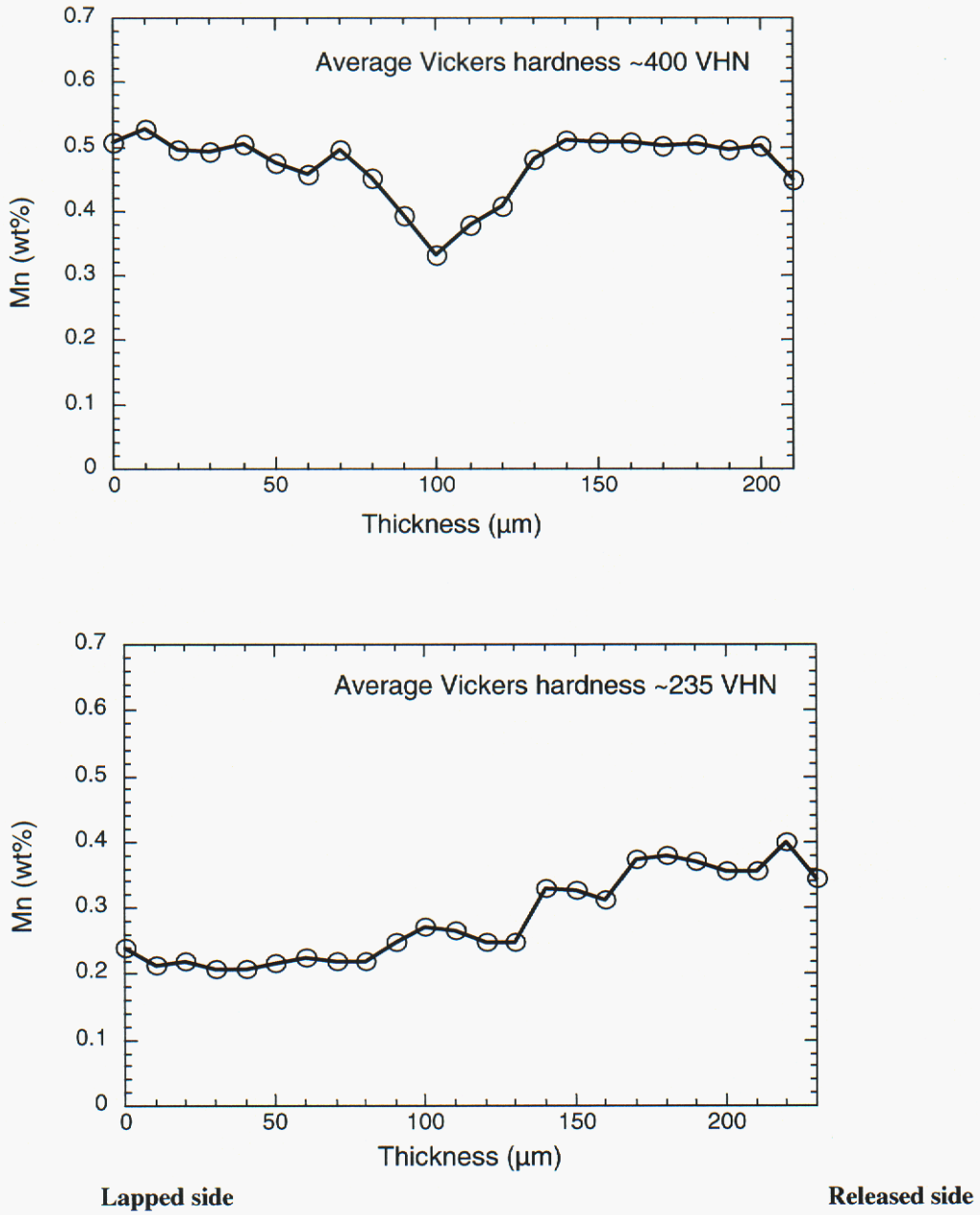


**Figure 7. Typical alloy composition profile through the deposit thickness.**
(a) - Uniform distribution of Ni-(0.5wt% Mn) except the middle thickness.
(b) - Mn concentration gradient through thickness

morphology and size. Grains were found to be needle-like with their long axis parallel to the PD and about 0.2-0.4 um wide (Fig. 8b). TEM/BF/DF images of the plan view show a high density of nano-scale twins (50-100nm wide) formed in the columnar grains (0.3-0.5um wide) (Fig. 8c,d). It is clear that these twins correspond to the cross section of the acicular features seen on the longitudinal cross section. It is also noticed that the acicular features vary in size from nano-scale to a few micrometer in scale

depending on the Mn concentration. For structures where the Mn concentration is less than 0.2wt %, the features are coarse and resemble the columnar grains observed in lot 13 of the Ni-sulfamate deposits.

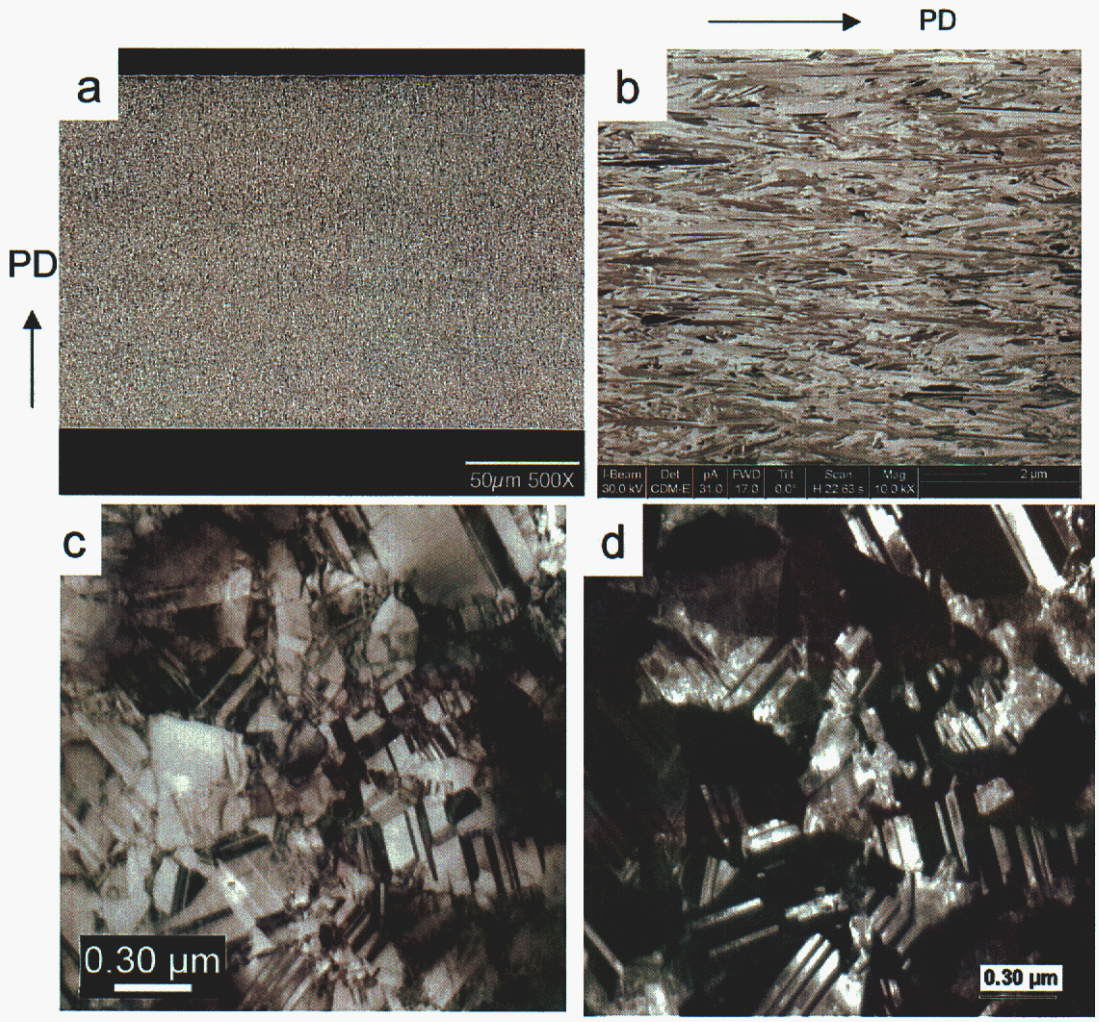


Figure 8. Typical microstructure of Ni-(0.5wt %) Mn revealed by (A) SEM/BEI (B) FIB images, and (C,D) plan viewTEM/BF/DF showing twins.

Vickers hardness

The measured Vickers hardness for the Ni-Mn (~0.5wt%Mn) was about 350-400 VHN. However, depending on the Mn concentration and grain size, the hardness could vary from ~220 to 400VHN. Generally, for deposits containing less than 0.2wt% Mn, the microstructure is coarse (>1.0micron) and soft (<300VHN). On the other hand, for deposit containing greater than 0.3wt%Mn, the microstructure is fine (<<1.0micron) and hard (>300VHN) as shown in Figure 9.

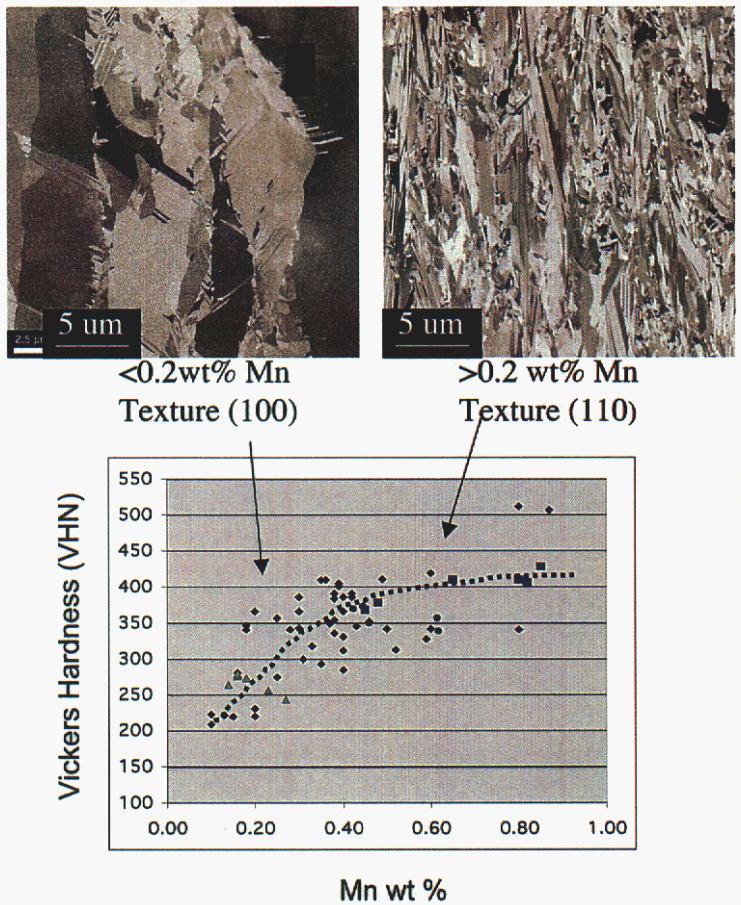


Figure 9. Correlation of Mn concentration, grain size and Vickers hardness for Ni-Mn structures.

Texture

Ni-(~0.5wt %) Mn generally possesses a moderate [110] texture along the plating direction. However, the texture orientations are greatly affected by the Mn concentration. The texture became [100] when the Mn concentration drops below ~0.2wt % as shown in the Figure 10.

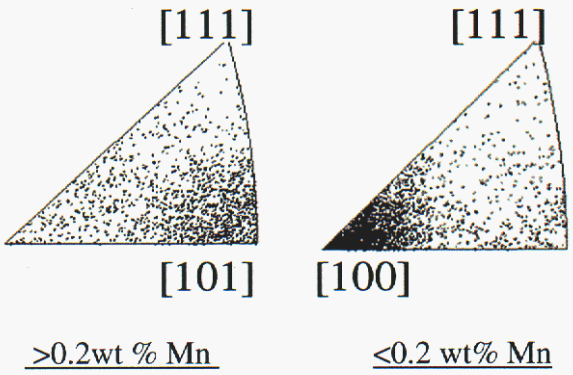


Figure 10. EBSP –derived texture orientation of Ni-Mn deposits; (left) high Mn (right) low Mn

(c)Ni-Co (30 wt %)

Ni-Co data are based mostly on electrodeposits (200um thick) plated on mold-free 1-inch Cu disks and on tensile bar test patterns.

Alloy composition and its uniformity

EMPA/WDS measurements show that the overall composition among the Ni-Co deposits can vary about ±10-15 % from the nominal composition (30wt% Co). In addition, composition variations through the thickness were observed. For the low aspect ratio mold-free deposit, Co concentration tended to deplete gradually toward the plating surface (Lapping side) as shown in Figure 11. The Co concentration near the lapped surface is about ~15% below the nominal concentration.

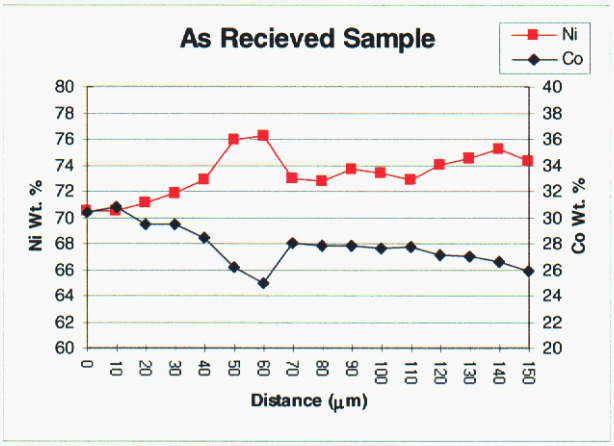


Released side Lapped side

Figure 11. Alloy composition profile through the thickness of the Ni-Co deposit.

Microstructure

SEM/BEI images show that the overall microstructural features of Ni-(30wt %) Co are relatively uniform through the thickness (Figure 12). FIB images show that the Ni-Co microstructure consists of submicrometer-size acicular or needle-like grains. These highly orientated grains were found to be about 200-400 nm wide. The acicular features are also revealed clearly by TEM/BF images. It is noticed that the width of these columnar features increases with a decrease in Co concentration (Figure 13).

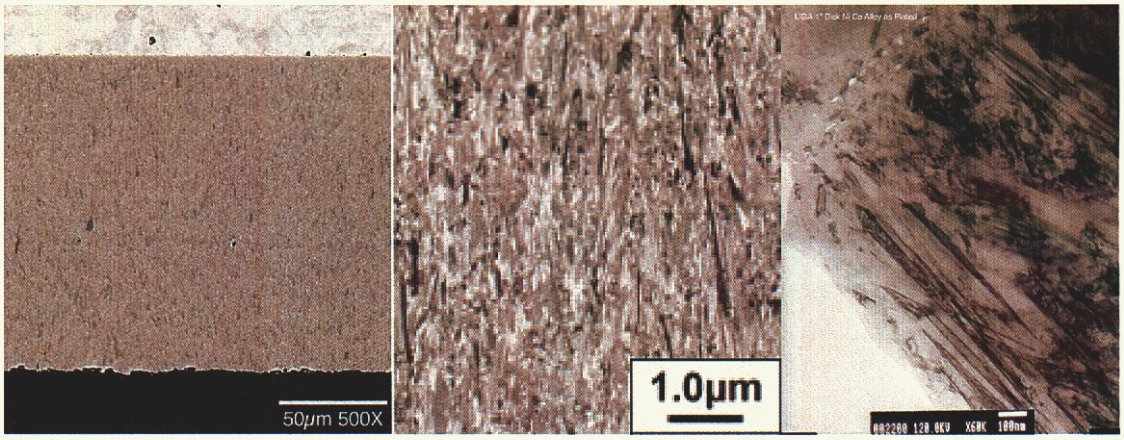


Figure 12. Typical microstructure of Ni-(30wt%) Co; SEM/BEI (left), FIB (center) and TEM/BF (right) images. Fine needle-like twins are revealed clearly in the TEM image.

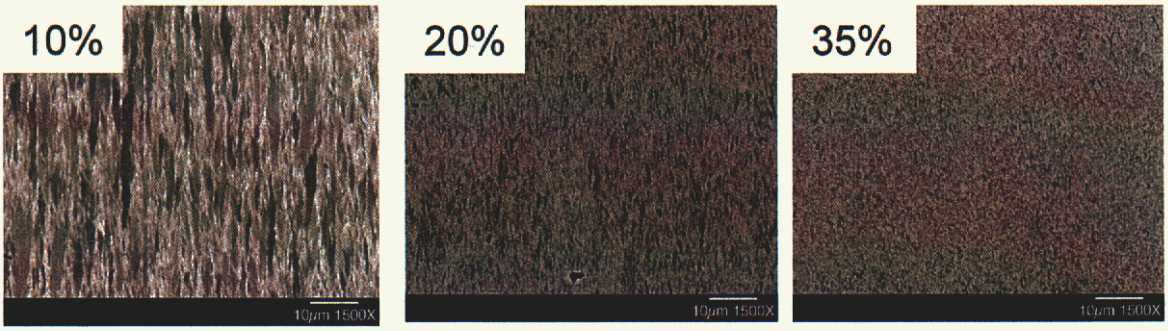


Figure 13. Microstructure feature size decreases with Co concentration.

Vickers hardness

Typical hardness of the Ni-Co (30wt %) deposits was determined to be 350-420VHN. The hardness appears to be greatly dependent on the alloy composition and grain size. Figure 14 illustrates the hardness increase with an increase in Co concentration and a decrease in grain size.

Texture

In general, Ni-Co deposits do not possess a texture as pronounced as those observed in the Ni-sulfamate and Ni-Mn deposits. In a few cases, the deposit showed slight signs of weak [110] texture as shown in Figure 15.

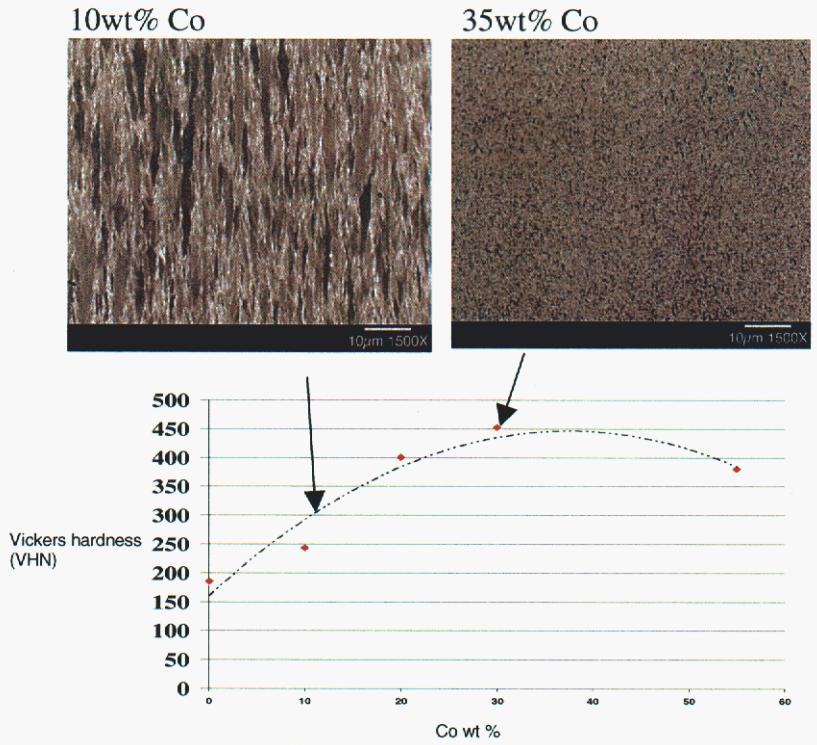


Figure 14. Correlation of Co wt %, grain size and Vickers hardness

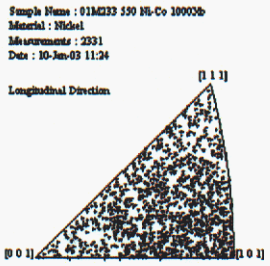


Figure 15. EBSP patterns show the weak, nearly random crystal orientation along the plating direction.

## (d) Ni-saccharin (stress relief additive)

Microstructure

Wet chemical analysis of the deposits showed that the deposits contained approximately 100ppm sulfur which is a characteristic element of the saccharin additive for stress-relief. Besides relieving the plating stresses, saccharin has been found to be an extremely effective grain refiner for the Ni-based electrodeposits. SEM/BEI images show the microstructural features of this deposit are extremely fine and too small to be resolved (Fig. 16). Both FIB and TEM/BF images show that the grain size is nanoscale,

< 100nm. Twinning in these nanoscale equiaxed grains is not as evident as observed for the Ni-Co and Ni-Mn alloys described earlier.

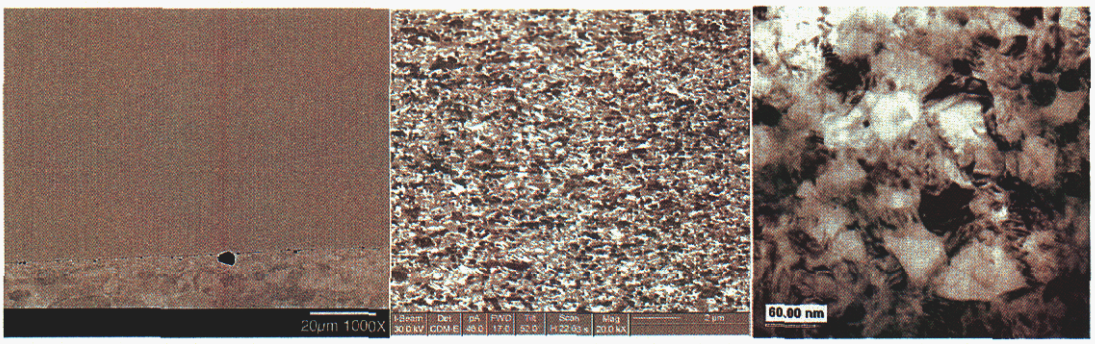


Figure 16. Typical microstructure of Ni-saccharin deposits.

Vickers hardness

The current Ni-saccharin electrodeposits were found to be extremely hard; 500-600VHN. These hardness values are quite consistent through the thickness in all the examined deposits.

Texture

XRD analysis showed that Ni-saccharin usually has a weak texture of (111). In many cases it contains bimodal texture orientations, a mixture of (111) and (311). EBSP analysis was not performed for these deposit due to the resolution limitation of the technique.

(iii) Thermal stability

In this study, the samples of the four baseline deposits were annealed in vacuum at 200C, 300C, 400C and 600C for one hour.

Microstructure and hardness

The plot of hardness vs. temperature in Figure 17 implies that the grain structure of Ni-30 Co and Ni-0.5Mn undergo little microstructural change when annealing at temperatures up to 300C for one hour. Figure 18 shows that the grain size of the Ni-0.5Mn electrodeposit is quite stable up to 600C. For Ni-30Co annealed at 600C, it is noticed that the grains began to coarsen from columnar to equiaxed (Fig 19). SEM/BEI images and knoop hardness measurements show a gradual increase in grain size and decrease in hardness toward the plating surface. As described previously the grain size and hardness gradient are the results of Co depletion through the thickness (Figure 11) and these gradients are amplified when subjected to annealing without significant modification of the compositional gradient, Figure 19. This means that the thermal stability of the Ni-Co deposit is greatly dependent on the alloy composition and existing gradients.

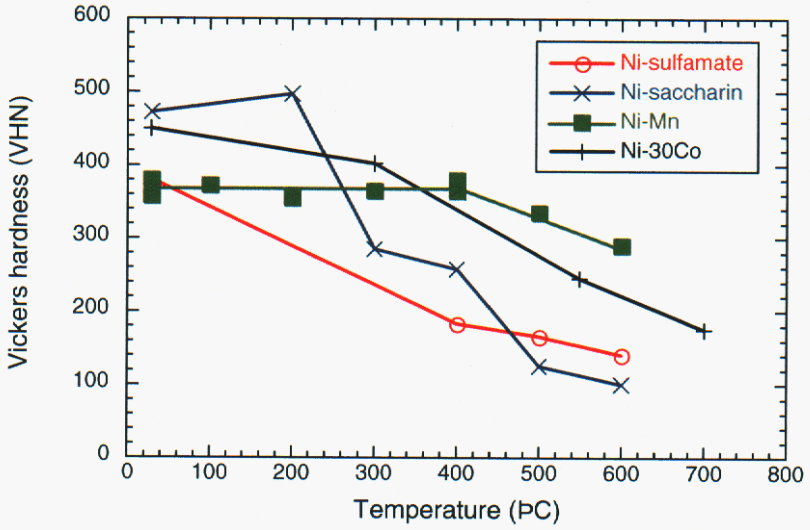


Figure 17. Effect of heat treatment on the Vickers hardness of electrodeposited materials

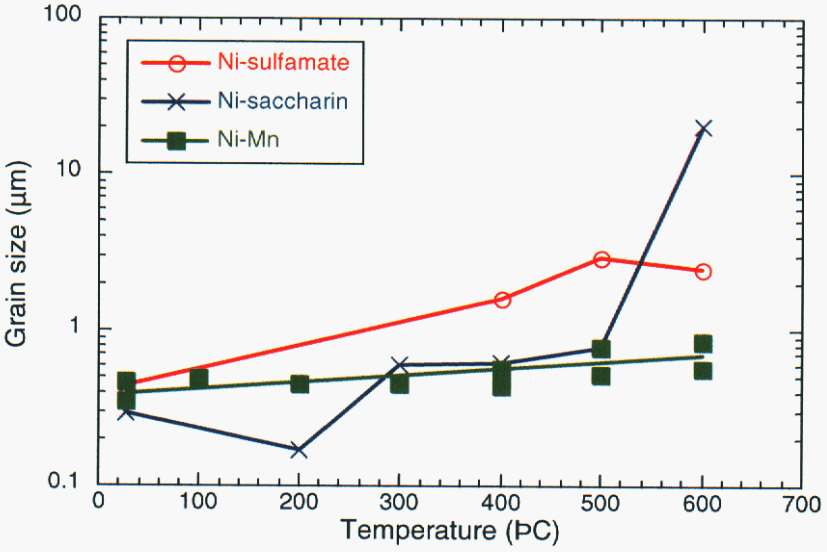


Figure 18. Effect of heat treatment on the grain size of electrodeposited materials

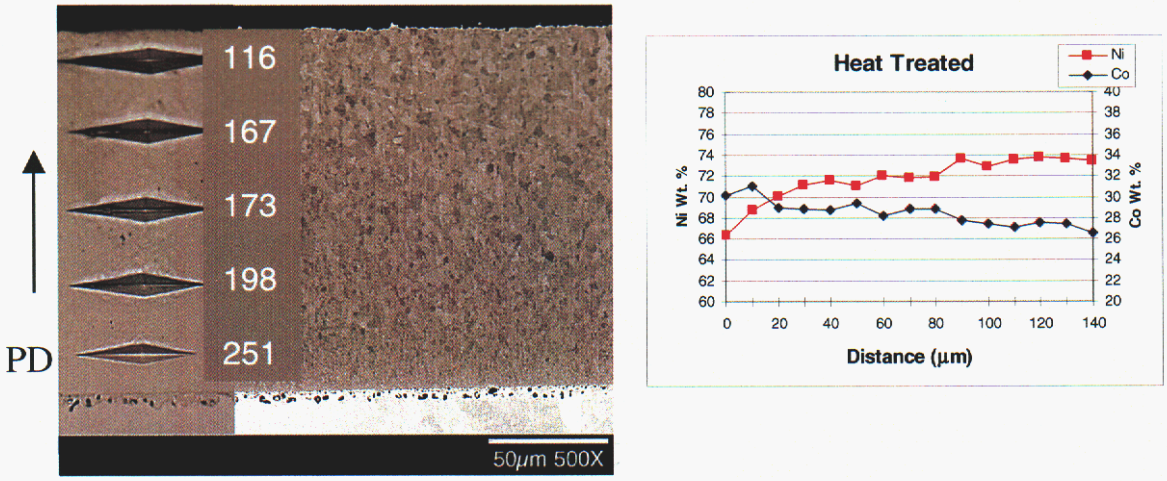


Figure 19. SEM/BEI image showing grain growth, grain size and Knoop hardness gradient through the thickness (a) and Co concentration gradient through the corresponding location (b).

The Ni-saccharin and Ni-sulfamate, on the other hand, are much less stable at these elevated temperatures. The nanoscale grains began to coarsen at temperatures as low as 250-300C (Figure 18) and the hardness drops dramatically, particularly for the Ni-saccharin, to levels similar to those of wrought Ni, i.e. ~100-120 VHN.

(iv) Surface finishing:

Released surface

SEM/SEI images show a variety of surface features on the released surface. These features range from smooth to pitted and stained from the etching step, and to replication of the Ti-Cu-Ti substrate surface (Figure 20).

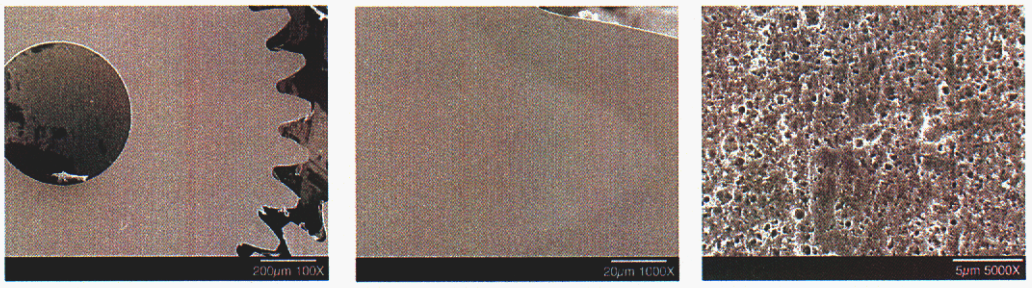

Figure 20. Release surface of LIGA gear

Lapped surface

SEM/SEI images show the lapped surface often contains machining marks from the mechanical lapping; pitting presumably from the relaease step; and/or porosity from the electrodeposition (Figure 21).

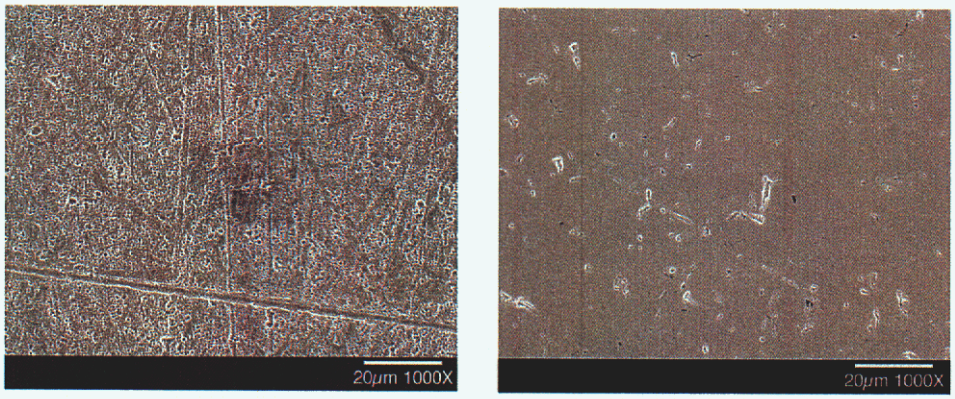


Figure 21. Lapped surface showing (a) machining marks and pitting, and (b) porosity.

Sidewall

SEM/BEI images (Figure 22) show three common surface features on the sidewalls. These features appear to be replicas of features seen on developed/etched PMMA molds.

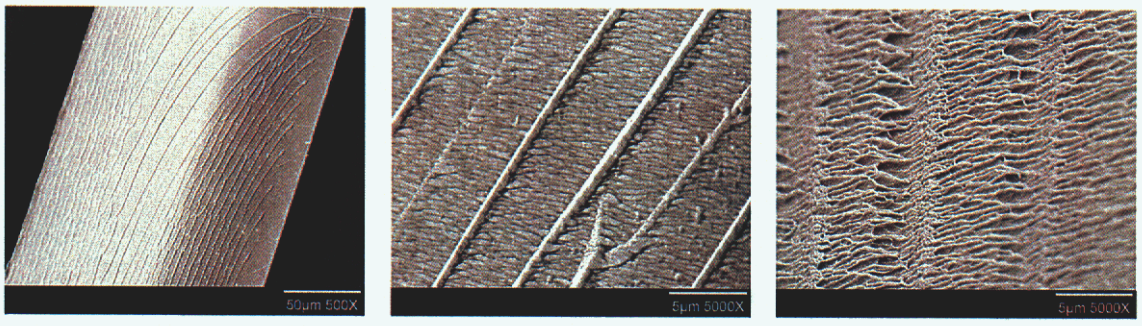


Figure 22. Sidewall features on electrodeposited Ni: river line patterns perpendicular to PD (left), fish scales (center) and grating lines paralleled to PD (right).

Sidewall of PMMA

There are three surface features similar to those seen on the deposit sidewall. The difference is that these features are topographically reverse from those on the electrodeposit sidewall. The horizontal river patterns on the PMMA mold are deep grooves, possibly cracks on the molds. The fish scale-like grooves are believed to be marks of the plasma beams from the deep etching. Similar patterns were also observed on the PMMA molds in etching experiments (Figure 23). The grating lines were also observed on the sidewalls of the PMMA mold and the Au-mask, suggesting that the grating lines originate from the Au mask, although the mechanism responsible for formation of these grating lines is unclear.

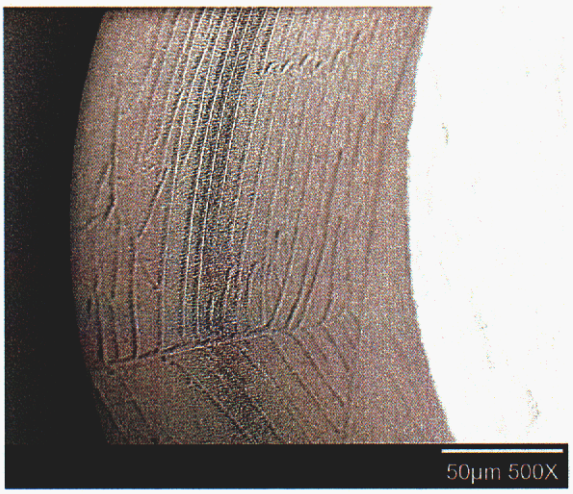


Figure 23. "River" patterns found on PMMA mold sidewall.

## Summary and Discussion

The most distinct characteristics of the baseline LIGA electrodeposits was found to be high strength and strong texture (or anisotropic). The key factors responsible for the high strength are the fine microstructure features at the nanometer- to submicrometer-scale. The factor affecting the texture (anisotropy)is not clear.

A challenge facing LIGA is to produce deposits with consistent and predictable metallurgical properties, and microstructure in particular. To achieve this goal, we placed the technical emphasis on understanding the microstructure and its association with other metallurgical variables. The major findings related to microstructure, texture, alloy composition, strength and their correlation are summarized in the following.

All LIGA baseline electrodeposits possess microstructural features and hardness that are at least 10 times smaller and 2-3 times harder, respectively, than those of wrought Ni. The microstructureal feature size, and consequently the hardness, are influenced greatly by the presence and concentration of alloying elements (Co and Mn) or impurities. Between the Ni-Co and Ni-Mn alloys, there is similarity in the correlation among Co or Mn concentration, grain size and hardness: the higher the Co or Mn concentration, the smaller the microstructure feature obtained and the harder the deposit becomes. A similar effect was also observed in the Ni-sulfamate deposit from Lot 13, where the metal impurity level is high.

The current study shows that the reduction of the microstructural feature size can be attributed mostly to an increase in twin density which reduces the effective grain size (Ref. 8-9). A mechanism for the twin's formation from the elemental addition is not clear. It is speculated that the twining results from a of lower stacking fault energy (SFE) due to Co or Mn or impurity additions (Ref. 10).

Anisotropy (texture) was found to be a characteristic of the LIGA electrodeposits. Texture orientation of the baseline LIGA materials appeared to vary with the alloying ingredient. A potential area for further research might be a determination of which factor(s) associated with an alloying element could affect texture orientation.

Our findings point to control of alloying elements or impurities as the key to success regarding the metallurgical consistency of the deposits. The critical issues needing to be addressed are an understanding of: a) kinetics and mechanism of the solute atom incorporation during the electrodeposition, and, b) how these mechanisms influence nucleation and grain growth of the deposits. Research efforts related to solute atom incorporation is being conducted by the computer modeling group in SNL (Ref. 11-13). The modeling hopefully will provide some guidance for producing LIGA deposits with suitable and consistent properties.

Thermal stability of the metallurgical properties does not appear to be an issue for Ni-Mn up to 500-600°C and for Ni-Co up to 300°C. The microstructure of Ni-saccharin, however, becomes unstable at temperatures higher than 300°C. Saccharin additions not only promote grain growth but also embrittle the boundaries due to sulfur segregation. Better understanding of the sulfur ion mobility in the electrolyte and the deposit should be an important task for future research.

Most surface features and irregularities on the LIGA deposit appeared to be process-related. The three features, river pattern, fish scales and grating lines, on the deposit sidewall are the replicas of the features on PMMA molds. Many of the process-related features may be eliminated by process modification. There is no evidence these surface features are metallurgy-related or are affecting the metallurgical properties.

## Conclusions

- The LIGA deposits are 2-3 time harder than those of the conventional wrought Ni. The high hardness is attributed to the submicrometer-size microstructural features with high twin density, which is a characteristic of baseline LIGA deposits.

- The concentration of alloying element, Co or Mn, plays a key role in controlling the microstructural feature size. For both Ni-Mn and Ni-Co deposits, there are strong correlations between the alloy composition, grain size, hardness and texture. Increasing Co or Mn concentration not only refines microstructural features but also modifies the texture orientation.

- Thermal stability of the metallurgical properties is an issue for the Ni-saccharin. The grains begin to coarsen at annealing temperatures less than 300°C. After exposure to elevated temperatures, the hardness of the deposit drops to levels similar to those of wrought Ni, ~100VHN.

- Surface finishing of the through mold deposits were mainly cosmetic and related to the process not metallurgy. There is no evidence that these surface features have any effect on the metallurgical properties.

## References


[1] Lin CS, et al. Materials Transactions, 2000;41:777.

[2] Yang NY, Kelly JJ. SAND Report, SAND2002-9311, July 2002

[3] Kelly JJ, Yang NY, SAND Report SAND2001-8609, October 2001

[4] Talin AA, et al. Poster Presentation for HARMST2003, Monterey, June 15-17, 2003.

[5] Lin CS, et al. Materials Transactions 2001;42:316.

[6] Malone GA. Plat. Surf. Finish. 1987;74:50.

[7] Kelly JJ, Goods SH, and Yang NYC. Electrochemical and Solid–State Letters 2003;6:C88.

[8] Reed-Hill RE., Abbaschian R. Physical Metallurgy Principles. Boston: PWS-Kent Publishing Co.; 1992. p. 556.

[9] Guy AG, Hren JJ. Elements of Physical Metallurgy. Menlo Park: Addison Wesley-Publishing Co.; 1974. p. 464.

[10] Chaduhuri DK, Xie D, Lakshmana AN. Wear 1997;209:140.

[11] Nilson RH., Griffiths SK. Journal of the Electrochemical Society. 2003;150(6):C401- 412.

[12] Griffiths SK, Nilson RH, Ting A, Bradshaw RW, Bonivert WD, Hruby JM, Microsystem Technologies, 1998;4:p.98.

[13] Evans GH, Chen KS, Larson RS, Greif R, Proceeding of 12th International Heat Transfer Conference, Grenoble, France, Aug. 18-23, 2002.

# Dormancy Effects in Parts Manufactured using the LIGA Process

## Introduction

Dormancy is a concern in LIGA parts for two reasons. First, bulk microstructural changes that may occur over time as a result of exposure to in-service environments could be expected to foster corresponding changes in mechanical properties and altered functionality of components. Second, the small feature size and high surface to volume ratio of LIGA structures leads to concerns that potential localized surface changes resulting from atmospheric exposure or surface contact between one LIGA part and another surface (LIGA or otherwise) may contribute to reduced performance. Accordingly, several different specimen geometries were exposed to controlled environments. Their surface appearances were examined before and after exposure, and both mechanical property and microstructural characterizations were performed and compared to the initial as-fabricated condition.

Only pure nickel structures (electroplated from a nickel sulfamate bath) were utilized in this experimental effort. Four different part geometries were used in this study; washers, gears, tensile bars and u-springs (Figure 1b-e), representing a range of anticipated structural requirements. Note that the teeth dimensions for both the u-springs and the gears are identical. The individual parts were distinguished by a simple numbering scheme: tensile bars are numbered in the 1000s, washers 2000s, gears 3000s and u-springs 4000s. Additionally, these parts came from six different lots of processed material, Table II.

## Experimental Procedure

A. Initial Characterization

The surface appearance of all specimens was documented prior to dormancy with an optical microscope. Digital images of the parts at low magnification (85x) were archived along with images at higher magnifications (up to 2614x) of distinguishing features such as scratches and processing artifacts. Primary attention was given to the lapped and release surfaces (during processing the lapped surface is prepared mechanically, denoted "L", and the release surface is prepared chemically, denoted "R"). The sidewalls were examined less systematically since these surfaces are not flat and thus high quality images cannot be obtained with standard light microscopy techniques.

B. Dormancy

Test chambers were designed and constructed to contain groups of LIGA specimens for controlled temperature and environmental exposures. After the initial visual examination, LIGA specimens were rinsed in acetone and methanol to remove possible contamination resulting from handling. They were then loaded in fixtures which maintained specific orientation and, where desired, controlled contact between a particular LIGA surface and another metallic surface. These contact surfaces consist of both LIGA/LIGA and LIGA/stainless steel combinations. After assembly, a fixture was loaded into a 304L stainless steel vessel (all fixture components were also constructed from 304L). The vessels were evacuated to a minimum of 10(-5) torr, then filled to a 0.5 psi positive pressure (over atmospheric) of gaseous nitrogen and sealed through the use of a valve. Two different sets of samples were prepared for dormancy testing; one set utilized a "dry" nitrogen mixture containing a minimal moisture level (-82°C dew point) and the other a "wet" nitrogen (-41°C dew point).

Figures 24 – 26 illustrate the hardware used in this study. One end of each tensile bar was clamped between two stainless steel washers; a stainless steel coil spring was used to apply the clamping force. The other specimen geometries (gears, washers and u-springs) were located on stainless steel posts that were pressed into holes drilled into the bottom washer. A bushing was placed on the center machine screw to prevent the top washer from contacting the LIGA parts (the top washer served only to prevent the LIGA parts from accidentally coming off their positioning posts during handling).

Nine pressure vessels were filled; these vessels are numbered C1 through C9 as listed in Table III. These vessels were then placed in a computer controlled temperature chamber and cycled between 70°C and –50°C, the duty cycle is shown in Figure 27. Two vessels, one with each environment, were removed after each of 90, 180, 365 days and 2 years (vessels designated for 2 years are due to be removed from dormancy in July 2004). The ninth vessel (dry nitrogen) was a control that was removed from dormancy after 30 days.

After dormancy, the surfaces were again examined and digital images were collected with a stereomicroscope. The stereomicroscope was chosen for the posttest images because it offered better lighting conditions and greater depth of focus, although at the cost of limits on magnification (only up to 150x). These posttest images concentrated on the same locations as for the pretest images except that the magnifications were generally limited to 150x. Additional images were taken with the optical microscope as deemed necessary for characterization of specific features; the higher magnification pretest images were not systematically reproduced posttest.

One posttest assembly (365 days, dry) was also examined by SEM in the as-assembled condition. After removal from dormancy, the top-clamping washer was removed and the bottom-clamping washer was placed in the SEM, with posts and parts remaining in the as-dormant position. After examining the top surfaces, the mount was tilted to provide a three-dimensional perspective of the contact regions. Then the legs of the u-

spring were lifted above the surface of the gear and washer so that the contact surfaces on all parts were exposed for further examination.

Tensile bars, both in the as-plated condition and after dormancy, were sectioned after fracture for microstructural analysis. Microhardness was measured at five points through the thickness of the polished cross-sections in the plating direction. SEM was used to reveal the grain structure and EBSD was used to identify the texture of the material in the plating direction.

C. Mechanical Testing

All tensile bars were loaded to fracture in a universal testing machine. Dormancy specimens are numbered 1xxx, and specimens in the as-plated condition are numbered 11xx. Strains were determined with a laser extensometer focusing on tape attached to the tensile bar at the extremes of the gauge section. Testing was performed at a constant crosshead displacement of 0.003mm/s, which corresponds to an initial strain rate of about $2x10^{-4}$ $s^{-1}$. Accurate modulus measurements could not be obtained with laser extensometry, therefore, a modulus of 200 GPa was assumed for yield strength determinations with an offset of 0.5% strain. The relatively large offset was chosen to accommodate the uncertainty of the strain measurement.

## Results and Discussion

A. General characteristics: Pretest

In general, the surface quality of the parts is characterized by the process lot from which they originate, although some surface features are common to all materials. Also the technique used to observe specific features can give starkly different impressions; for example, slight perturbations in the flatness of the surface are accentuated by stereomicroscopy methods, while the same feature may be nearly indiscernible by optical microscopy since the focal length is narrow with this technique.

*Tensile bars*

The release side typically has circular features that appear to be raised from the surface, these features are often located near corners and may be over 100μm in diameter, Figure 28. Additional features on the release side appear as patterns reminiscent of aerial photos of flooding erosion, Figure 28; these are called here river patterns. These river patterns range from uncommon (lot 14/31-306) to a distinguishing characteristic of some lots (13/36-351) that may cover much of the release surface. The lapped surfaces have scratches, Figure 28, presumably from the lapping stage: in some lots scratches may be nearly indiscernible (14/31-306), while on others scratching may be heavy and be attendant to stains that appear to be residue from final lapping or subsequent cleaning stages (13/36-351 and 13/36-352).

Tensile bars from lot 31-306 qualitatively appear to have the cleanest lapped and release surfaces. Parts from lot 31-307 have some scratches on the lapped surface, presumably from the lapping step. The lapped surfaces of parts from lot 36-351 are characterized by significant density of scratches and stains, while the release surface shows extensive river patterns. Lot 36-352 displays the most significant scratching on the lapped surface of any of the materials. These observations are summarized in Table IV.

*Subassembly parts: washers, gears and u-springs*

The subassembly parts, washers, gears and u-springs, are derived from different processing lots than the tensile bars and have some different features; for example, stains were not observed on the subassembly parts. The lapped surface of parts from lot 14/30-291 have black spots which were subsequently determined by SEM in the posttest condition to be porosity, Figure 29. This porosity appears irregular in shape, up to 1μm in largest width, and widely dispersed having a density of greater than 50 pores per 2500 $\mu m^2$. These pores give the impression of space between columnar grains since they often appear triangular on the surface. No surface porosity has been observed in the other lot of subassembly parts (13/30-300), nor on the tensile bars. The release side of the subassembly parts shows raised circular features often associated with modest river patterns around these features, Figure 30. The release side also appears to have a matte surface in images from the stereomicroscope, while in posttest images from SEM, these surfaces appear to have a submicron finish. The u-springs, in particular, display a seemingly unique feature: a raised area on the release side of each tooth (and occasionally a few in other locations on the release side), Figure 31. These features appear to be raised from the surface with a slightly recessed top like a volcano as shown in cross section in Figure 31b. These features are not always in the same position in the tooth and the recessed region appears quite rough.

The sidewalls were not examined systematically, in part because many of them are curved hence difficult to examine. In a few cases where the sidewalls of curved surfaces were examined, the sidewalls have a series of in-plane bumps extending around the circumference of the part, Figure 32. These bumps do not cover the entire sidewall, rather a band of bumps exists usually extending from the release side to somewhere near the middle of the thickness.

B. Assembly Contacts

SEM of the assembly showed that close contact was made between the teeth of the gears and the u-springs, as well as on the flats between the washers and u-springs. Structural changes at these contacts were not evident: the definition of the parts and corners remained distinct and well-defined, Figure 33. Upon disassembly the contact surfaces appeared to be unchanged. Comparison of sidewalls at contacts and away from the contacts, in particular the bumps on the sidewalls, showed no clear changes, Figure 34.

C. Comparison Pretest and Posttest

Comparison of pretest and posttest images does not show a significant difference for any of the observed parts. Since SEM of the parts before dormancy was avoided, we do not have high magnification images in the pretest condition. The lapped and release sides of several parts both pretest and posttest are presented in Figure 35. The majority of the surface features can be tracked from pretest to posttest images collected from the light microscopes. The porosity, for example, which was revealed by SEM on posttest images of the lapped side of parts from lot 14/30-291, Figure 29, was present pretest: the dark marks revealed in the light microscopy correspond to these pores and are present in both pretest and posttest images.

Additional scratches are often present on posttest specimens due to handling, but there are few, if any, unaccounted features present on the posttest images. The only obvious features apparent on the surfaces of the dormancy specimens posttest are marks that appear to arise from condensation in C8, i.e. wet nitrogen in dormancy for one year, Figure 36. These water marks are located on the tensile bars near the end where they are clamped. There is no evidence that these marks are more than superficial.

It should also be noted that in one case it was found that metal flakes were embedded in the release surface of a tensile bar as shown in Figure 37. The flakes appear to be steel, probably stainless steel since they are rich in Fe and Cr (as determined by EDS). The source of these "flakes" remains unknown, but they did not seem to affect the mechanical properties of tensile bar 1041 where they were observed.

Tensile bars, both in the as-plated condition and after dormancy, were sectioned after fracture for microstructural analysis. Fig. 38 shows that the pretest and posttest microstructures compare favorably for materials from the same lot. The grain sizes are difficult to determine from these SEM images, but it is clear that the average grain size is different among the various lots of materials. Moreover, the general trend of smaller grain size, greater strength is followed as summarized in Table VI and the following section. It should also be noted here that the grain size varies with aspect ratio such that the grain size may change from the root of a gear tooth to the end (or outside edge) of a gear tooth; consequently the properties of the electrodeposited material in the region of a bearing surface may differ from the "bulk" properties of the part.

D. Mechanical Testing

The results of the tensile tests are summarized in Table V. The stress-strain curves for the as-plated specimens (11xx) are plotted in Figure 39. This plots shows that the strength varies from lot to lot of electrodeposited material. The measured stress-strain curves for materials that have experienced dormancy are plotted in Figure 40 a-d by processing lot. It is apparent from comparing these figures that the differences between the lots are larger than the scatter within each individual lot. This essential feature of these flow curves is evident in Figure 41, a plot of the ultimate tensile strength as a function of uniform strain: (i) the data clearly cluster by lot independently of the

dormancy parameters, and (ii) the properties of the as-plated and dormancy specimens appear to the be indistinguishable. Examples of the fracture surfaces are shown in Figure 42 for the as-plated condition and in Figure 43 for the dormancy material. Again, the trends are distinguished by the material lot rather than the dormancy parameters. In summary, the evidence indicates that the mechanical properties are unchanged by the duty cycles up to a year in dry nitrogen and in wet nitrogen. The tensile data is summarized in Table VI.

The uniform strain (strain at peak load) is relatively low for these materials, less than 4% for the lots of material from tank 13, but between 4 and 6% for the lot of material from tank 14. Estimates for the reduction in area, however, range from 60 to 70% for the materials from tank 13 and are much higher for the materials from tank 14. In general, material with the lowest ductility exhibit the highest strength values according to processing lot as summarized in Figure 41, The differences in mechanical properties from one lot to the next is believed to be a consequence of texture in these materials, as the microstructural texture of the tensile bars differs between lots as shown in Figure 44. This variation in texture also explains the anisotropic necking behavior observed in Figures 42 and 43.

Microhardness measurements bear the same trends: the microhardness before and after dormancy is the same within the scatter of the data for a given lot. The four lots of material, however, differ significantly one from the other. It is interesting to note that the strongest lot of material is not the hardest, although the hardness between the two strongest materials is relatively close considering the inherent scatter in hardness data. Generally, these two properties follow one another, and the reason that they do not, in this case, is unclear.

E. Dormancy: Two Years

Samples that will experience dormancy for two years will be removed from the test chamber in July 2004.

## Conclusions

The following conclusions were made regarding the controlled dormancy exposures of nickel-sulfamate LIGA specimens:

- Surface appearance of nickel-sulfamate test specimens remains relatively unchanged after periods of up to one year in dry nitrogen. Both lapped and released sides appeared unchanged (neglecting marks resulting from handling) after testing.

- Some specimens exhibited surface staining after exposure to a "moist" nitrogen environment. These features are attributed to the presence of condensation during thermal cycling; however there is no indication that any significant metallurgical events have occurred in those regions.

- Close examination of LIGA surfaces that were in contact during dormancy testing did not reveal the presence of any localized chemical changes, regardless of the contact material (LIGA or stainless steel).

Mechanical testing of as-plated specimens revealed differences in behavior which are consistent with microstructural differences found in electrodeposits made from two different plating tanks. However, hardness, tensile strength and tensile ductility were consistent within a specific lot of material, and unaffected by dormancy exposure.

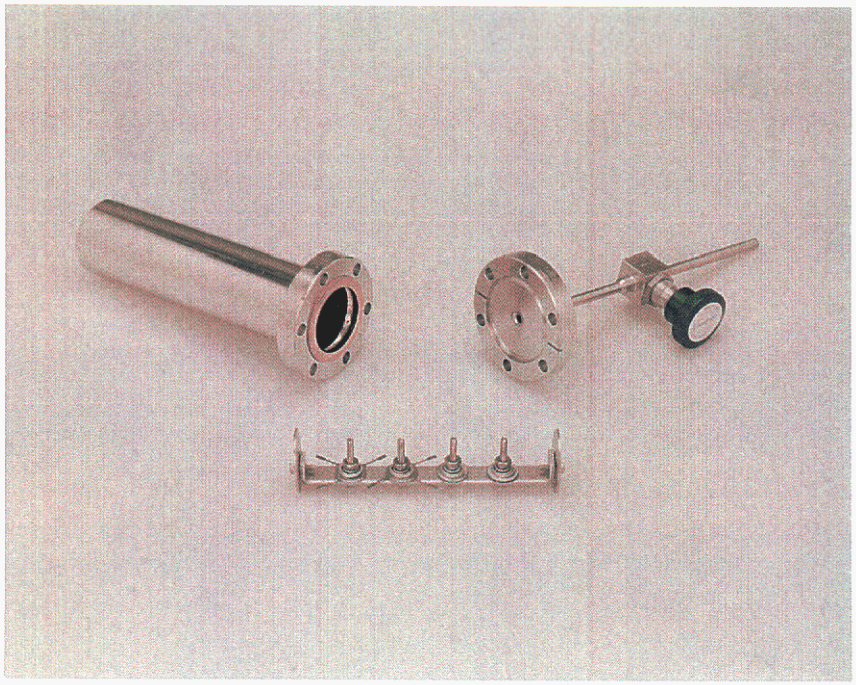

Figure 24. Holding fixture and container used for dormancy testing.

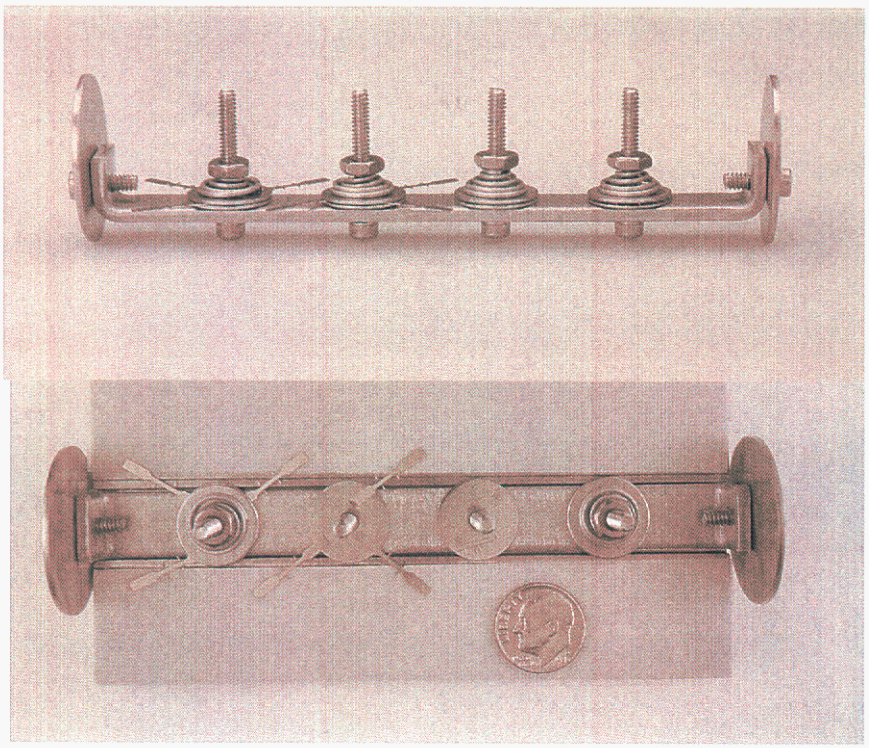

Figure 25. Side (top) and plan view (below) of clamping fixture used to hold test specimens.

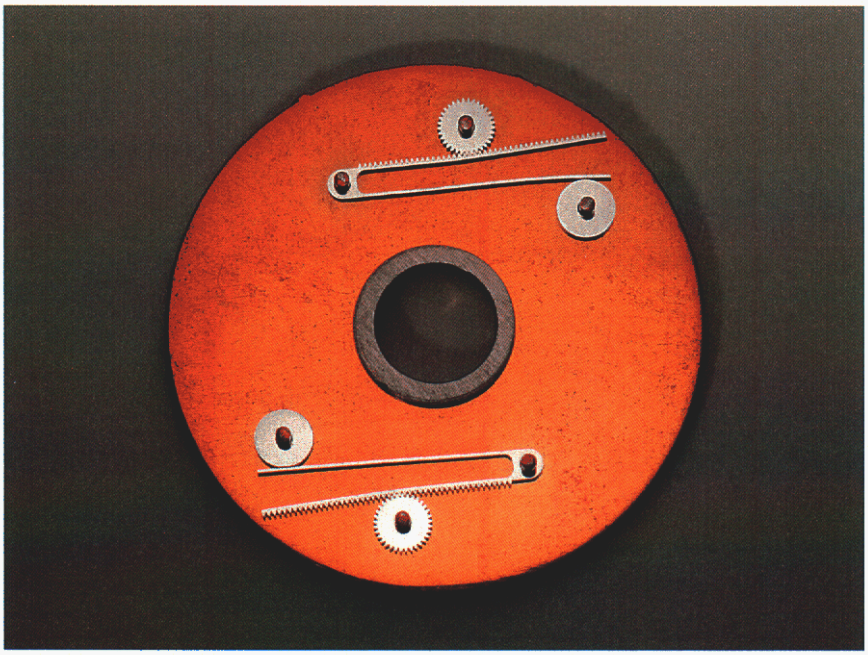

Figure 26. Close-up view of gear / u-spring / washer positioning used in dormancy testing.

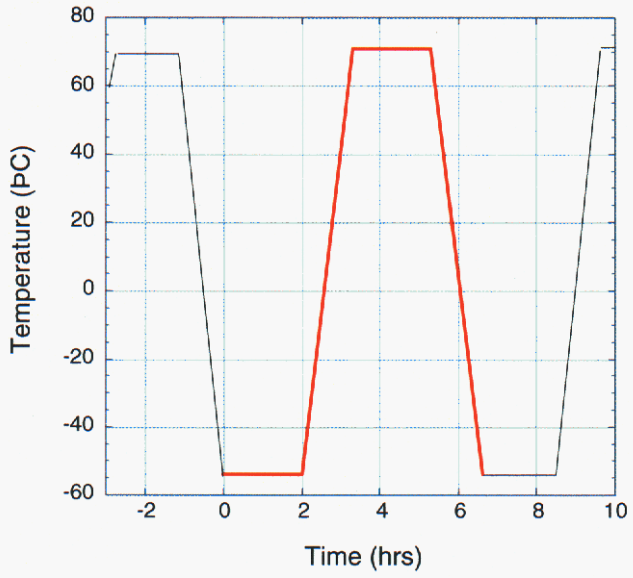


Figure 27. Temperature profile of thermally cycled dormancy containers.

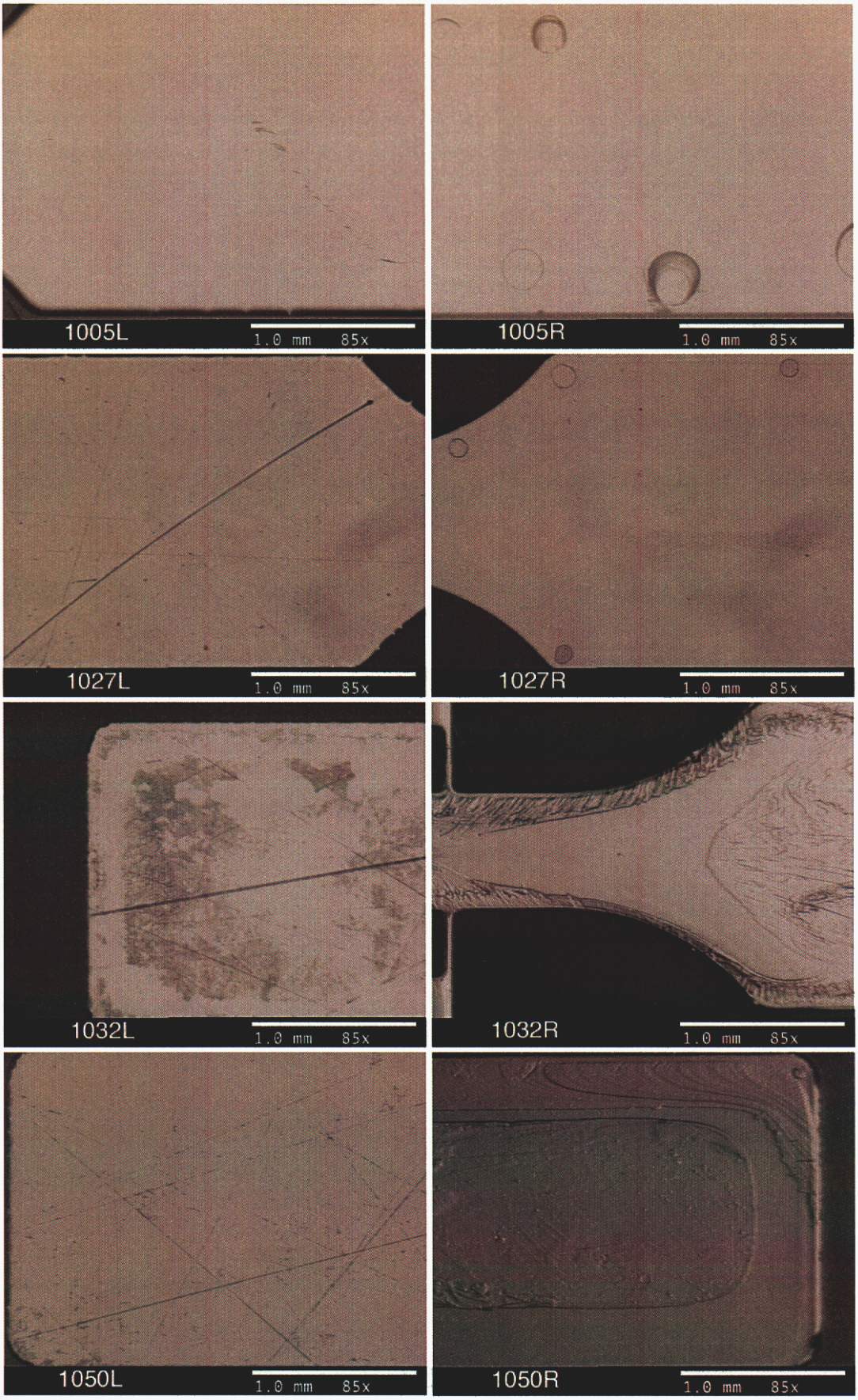


Figure 28. Lapped and release surfaces of tensile bars from four lots of materials: (a) 14/31-306, (b) 13/31-307; (c) 13/36-351; and (d) 13/36-352.

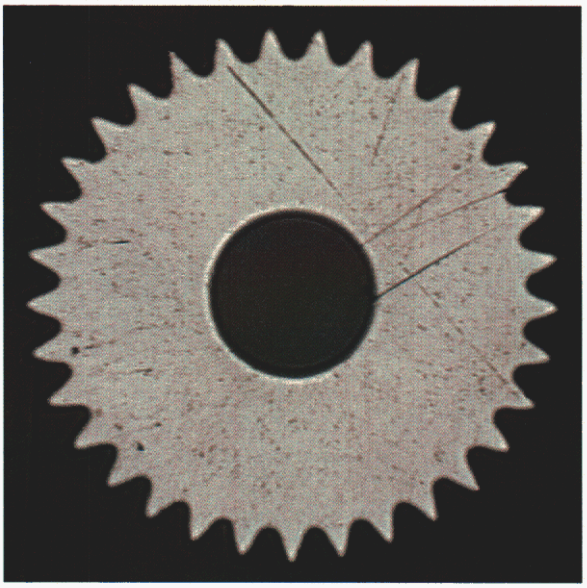

(a)

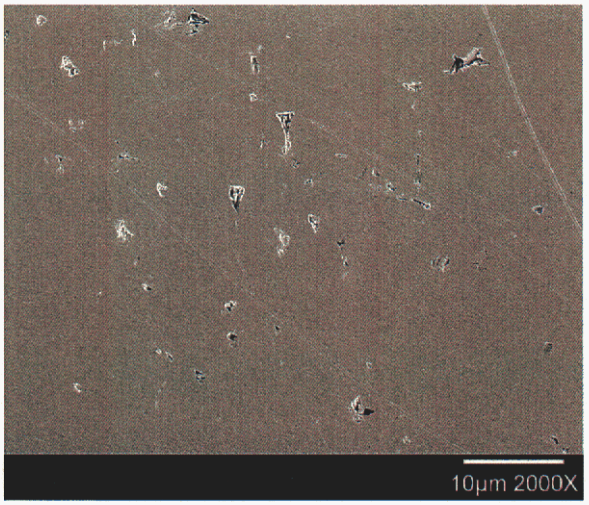


(b)

Figure 29. Specimen 3013L showing scratches and a high density of black marks (a) that are observed to be pores at high magnification (b).

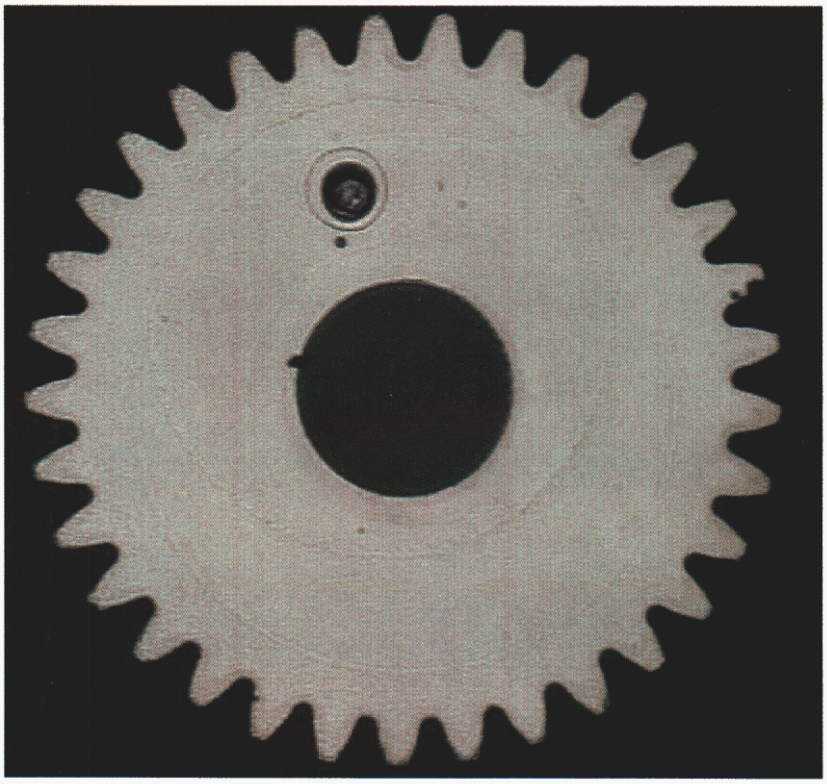

Figure 30. Specimen 3013R showing the general character of the release side of a gear.

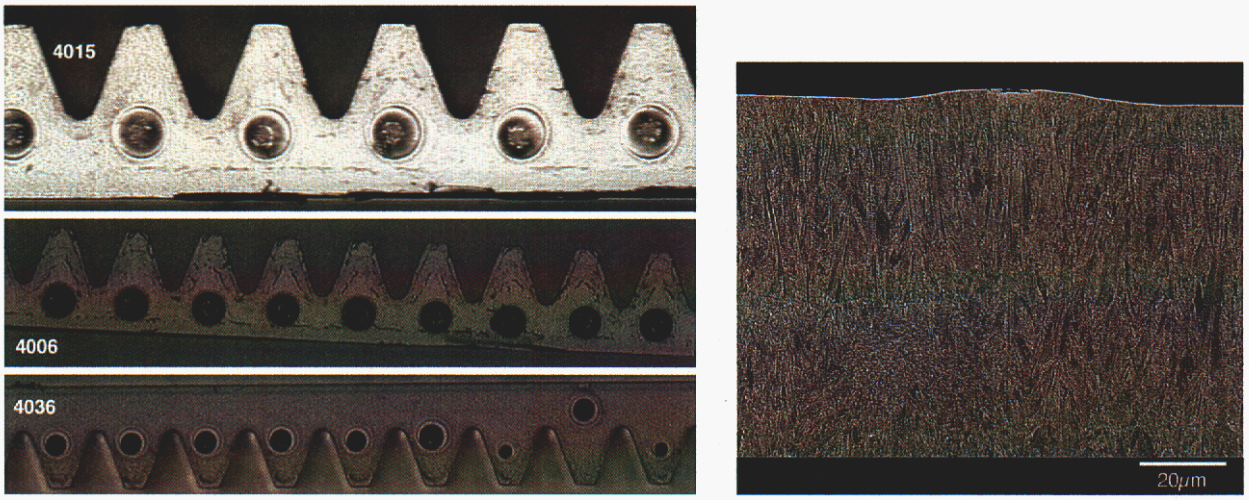


Figure 31. Stereomicroscopy images of the "buttons" on the release side of several u-springs (left), and cross section through a button on u-spring 4040 showing height of the button (approximately 3 μm) and recessed top (right).

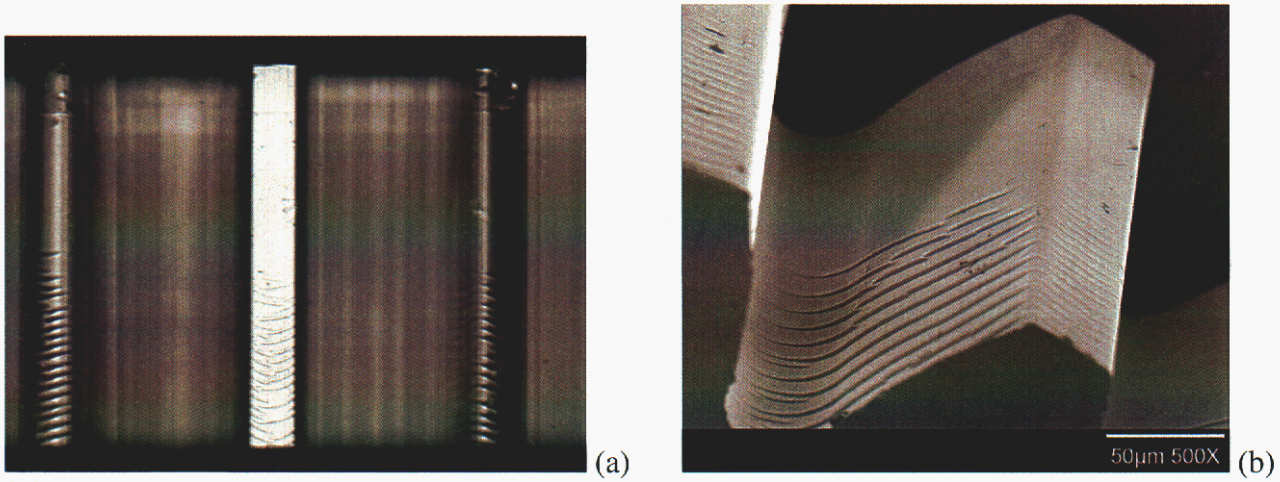


(a) (b)

Figure 32. The "bumps" on the sidewalls of gear 3039, optical image (a) and gear 3006, SEM image (b).

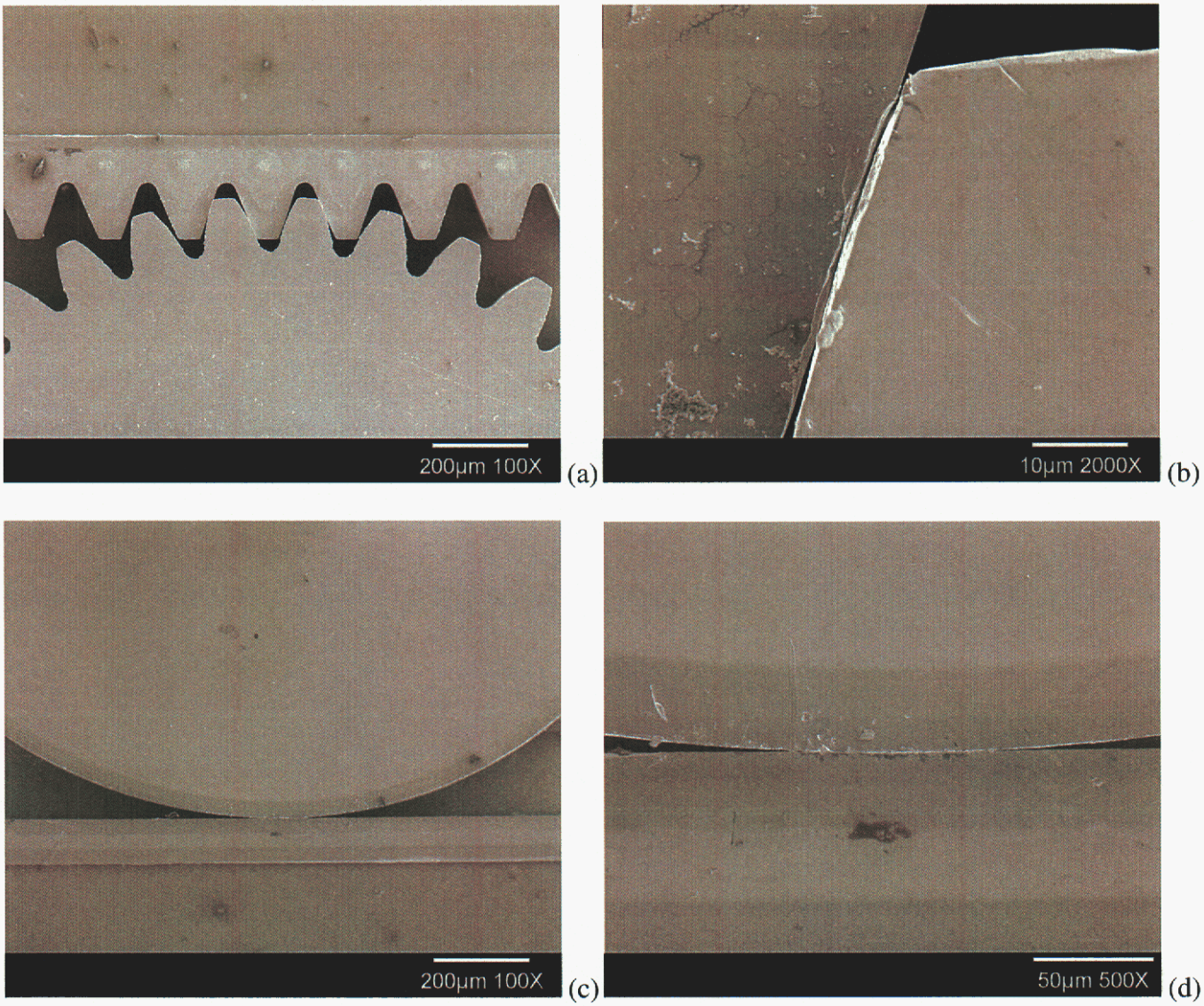


Figure 33. Contact between a gear (3006) and u-spring (4006) (a,b); and contact between a washer (2007) and u-spring (4006) (c,d).

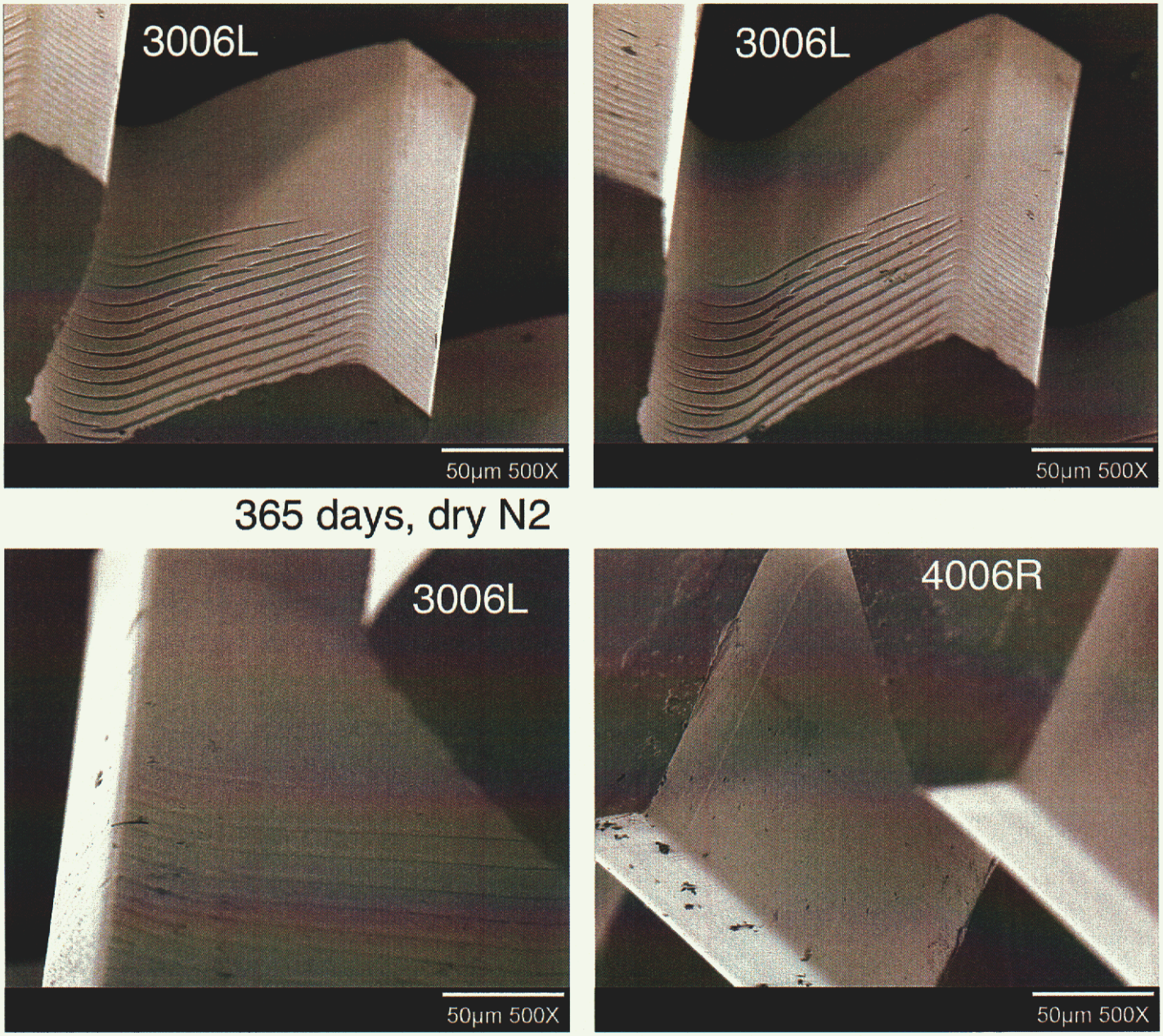


Figure 34. Contact surfaces after disassembly.

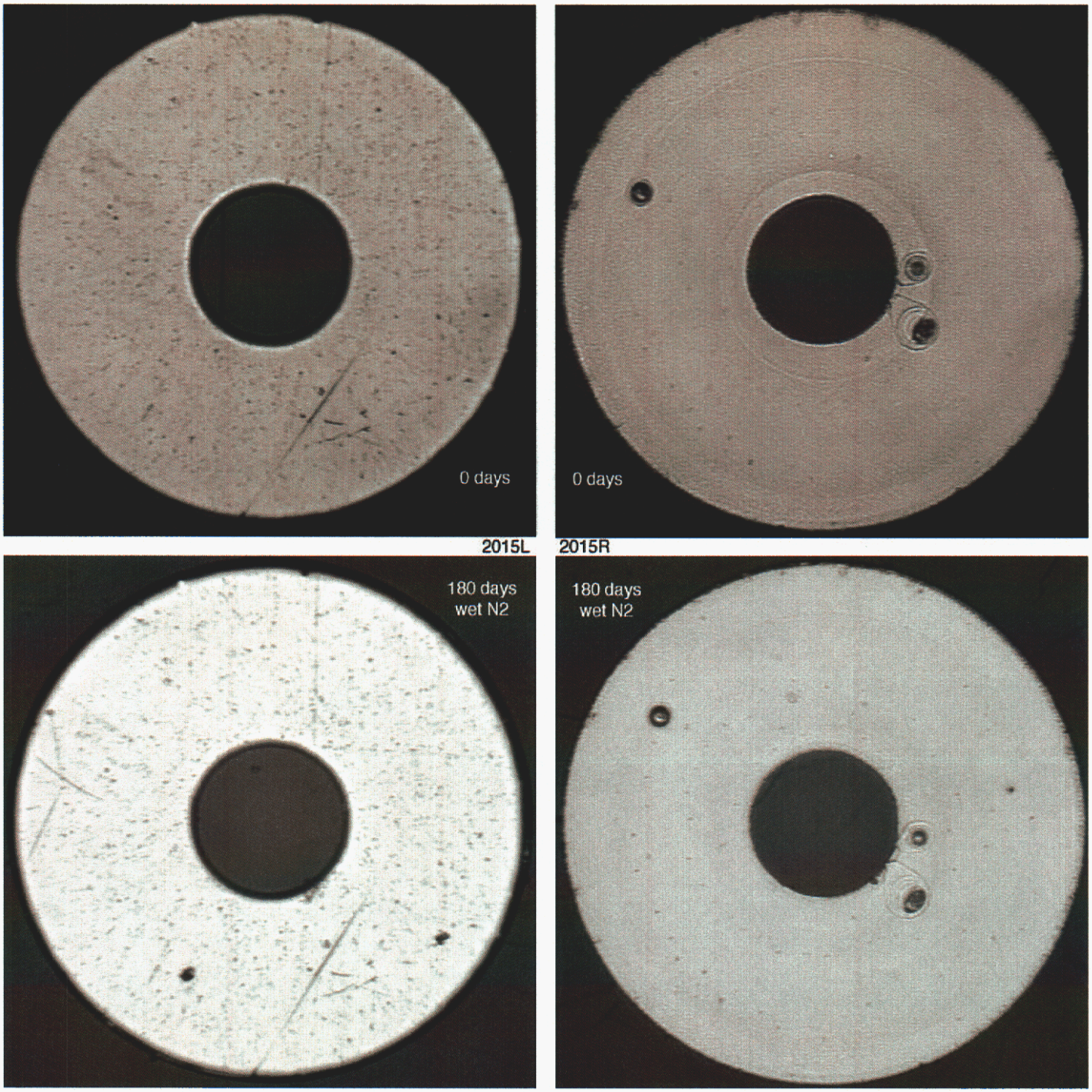


(a)

Figure 35. Images before and after dormancy for (a) washer 2015, (b) gear 3014, and (c) u-spring 4014.

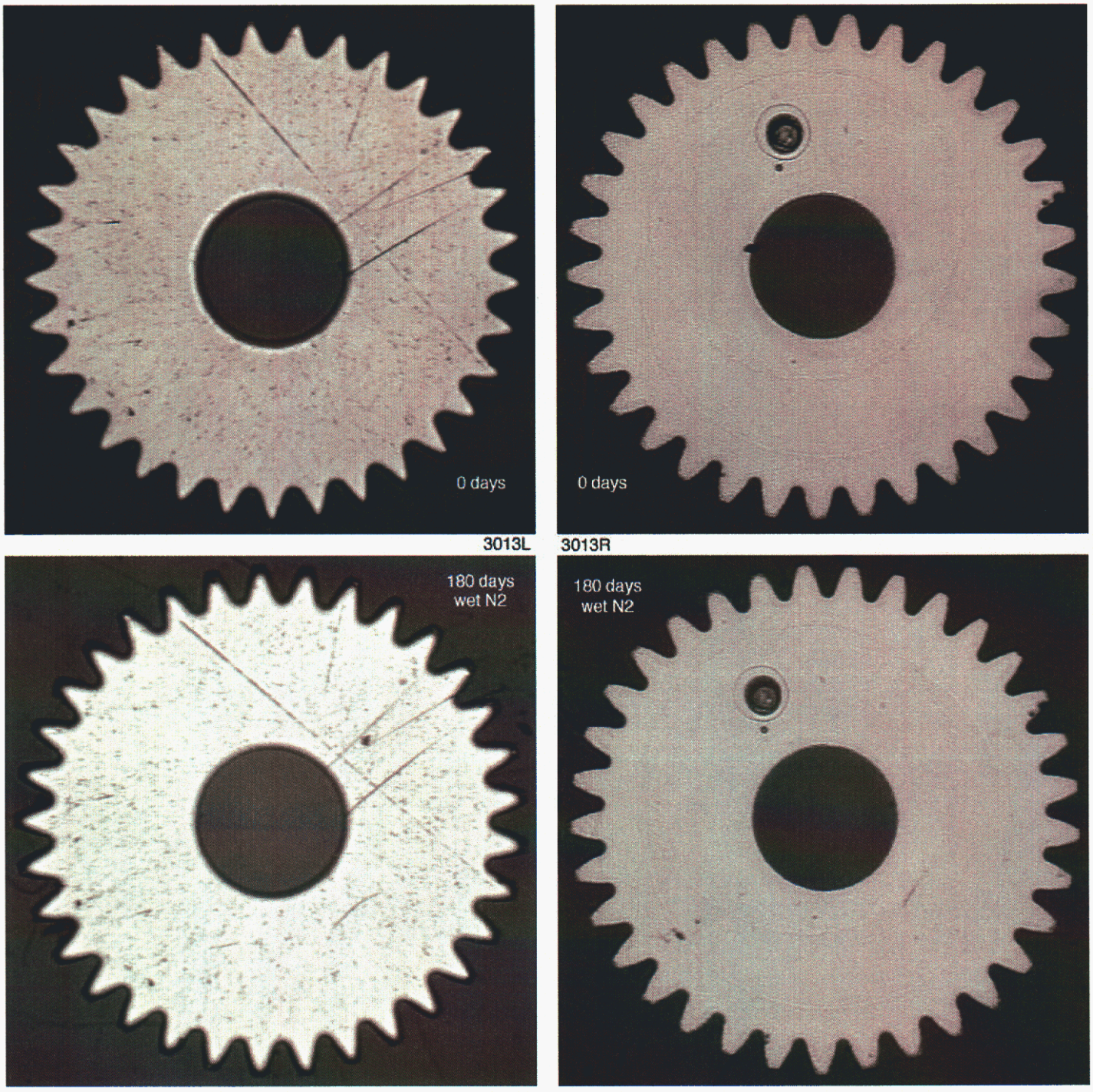


(b)

Figure 35. Images before and after dormancy for (a) washer 2015, (b) gear 3014, and (c) u-spring 4014.

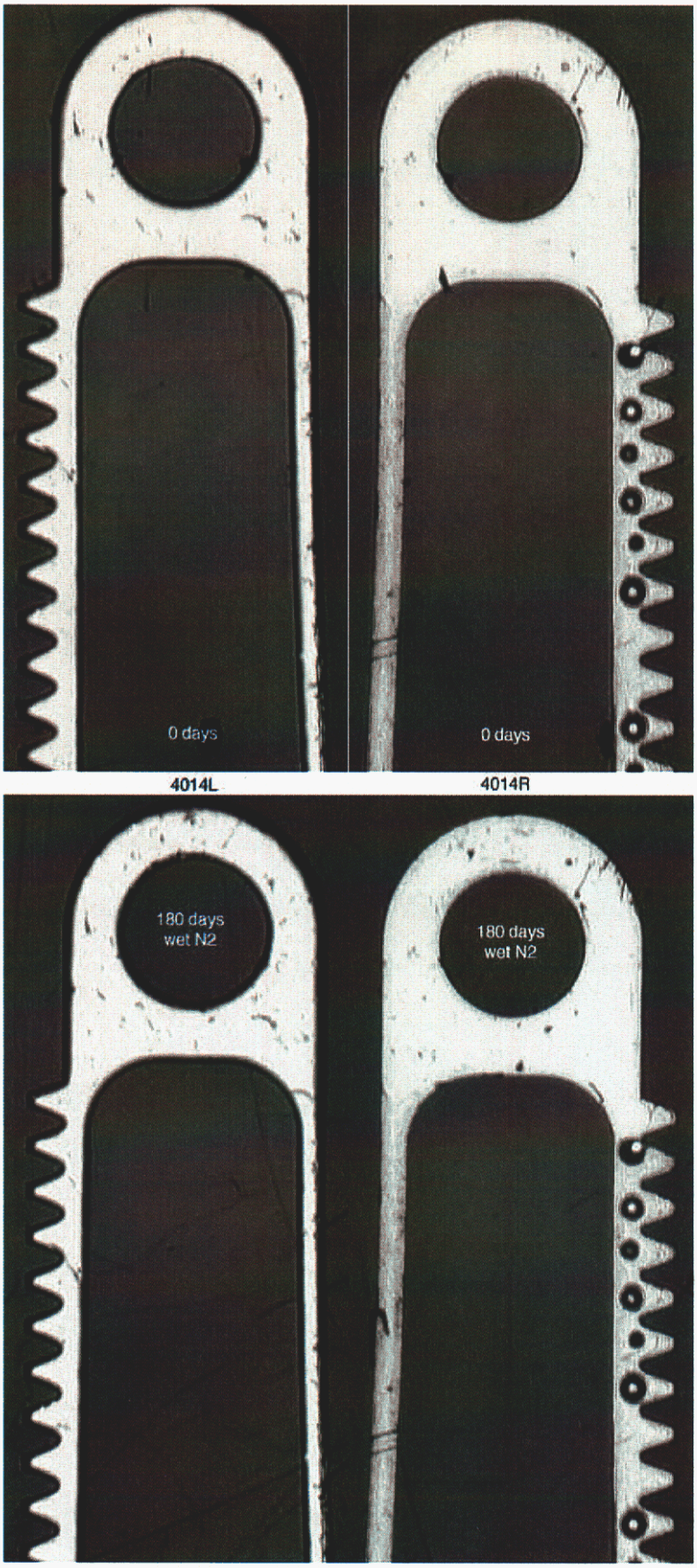


(c)

Figure 35. Images before and after dormancy for (a) washer 2015, (b) gear 3014, and (c) u-spring 4014.

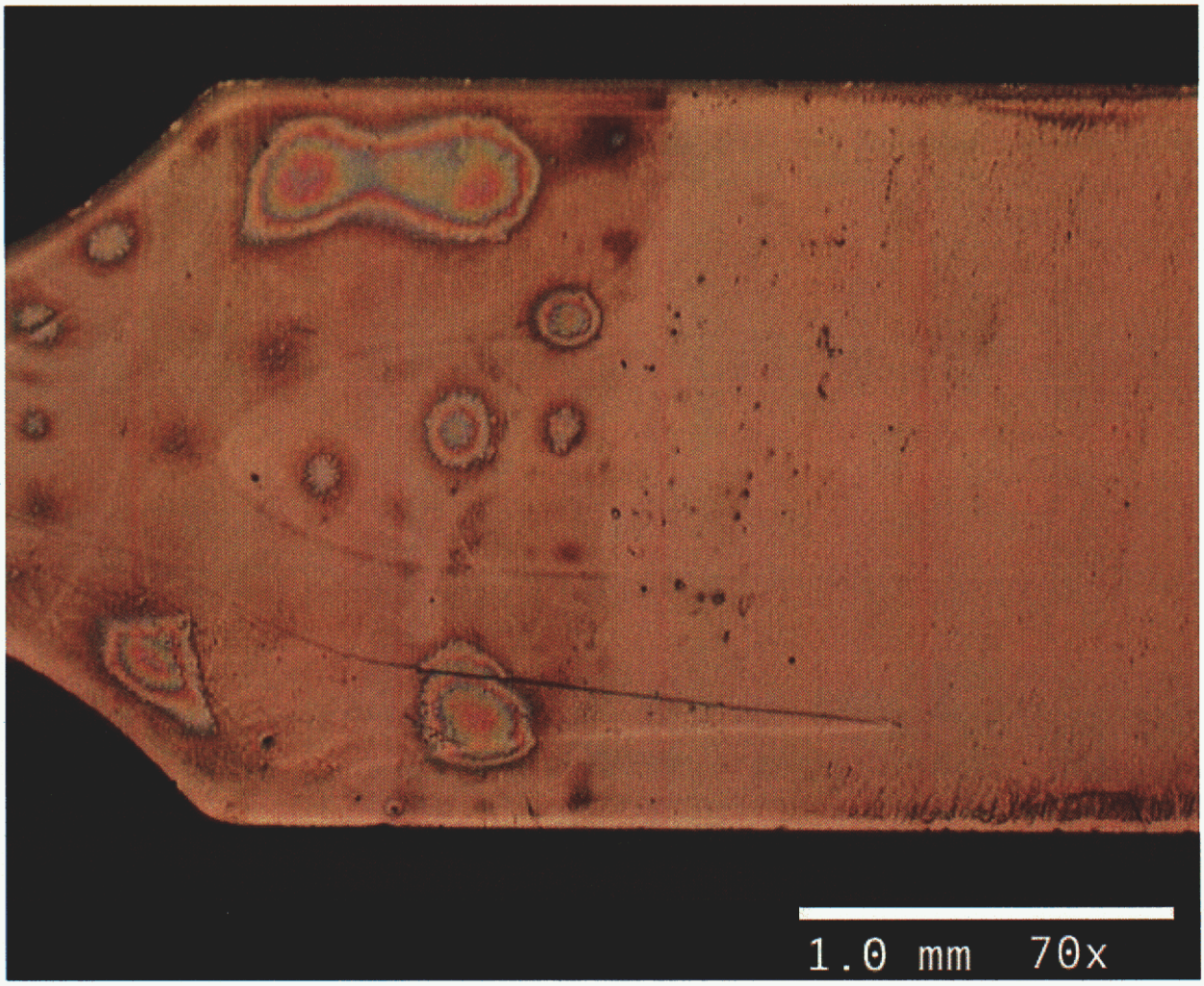


Figure 36. Water stain on tensile bar after 1 year in wet nitrogen.

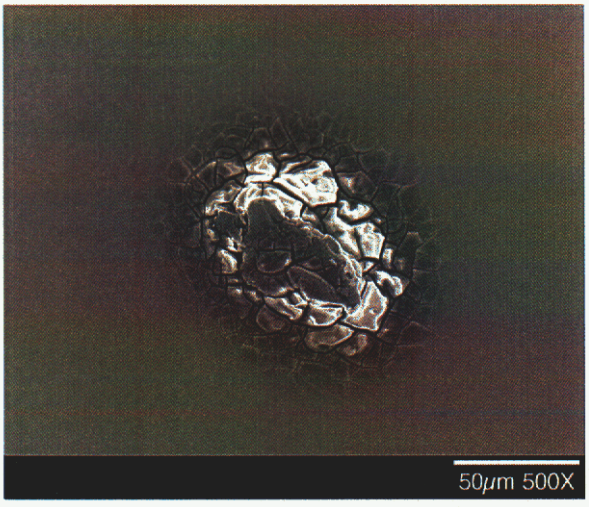


(a)


(b)

Figure 37. Flakes of material embedded in the release side of tensile bar 1041; these flakes are thought to be steel since EDS reveals that they are rich in Fe and Cr.

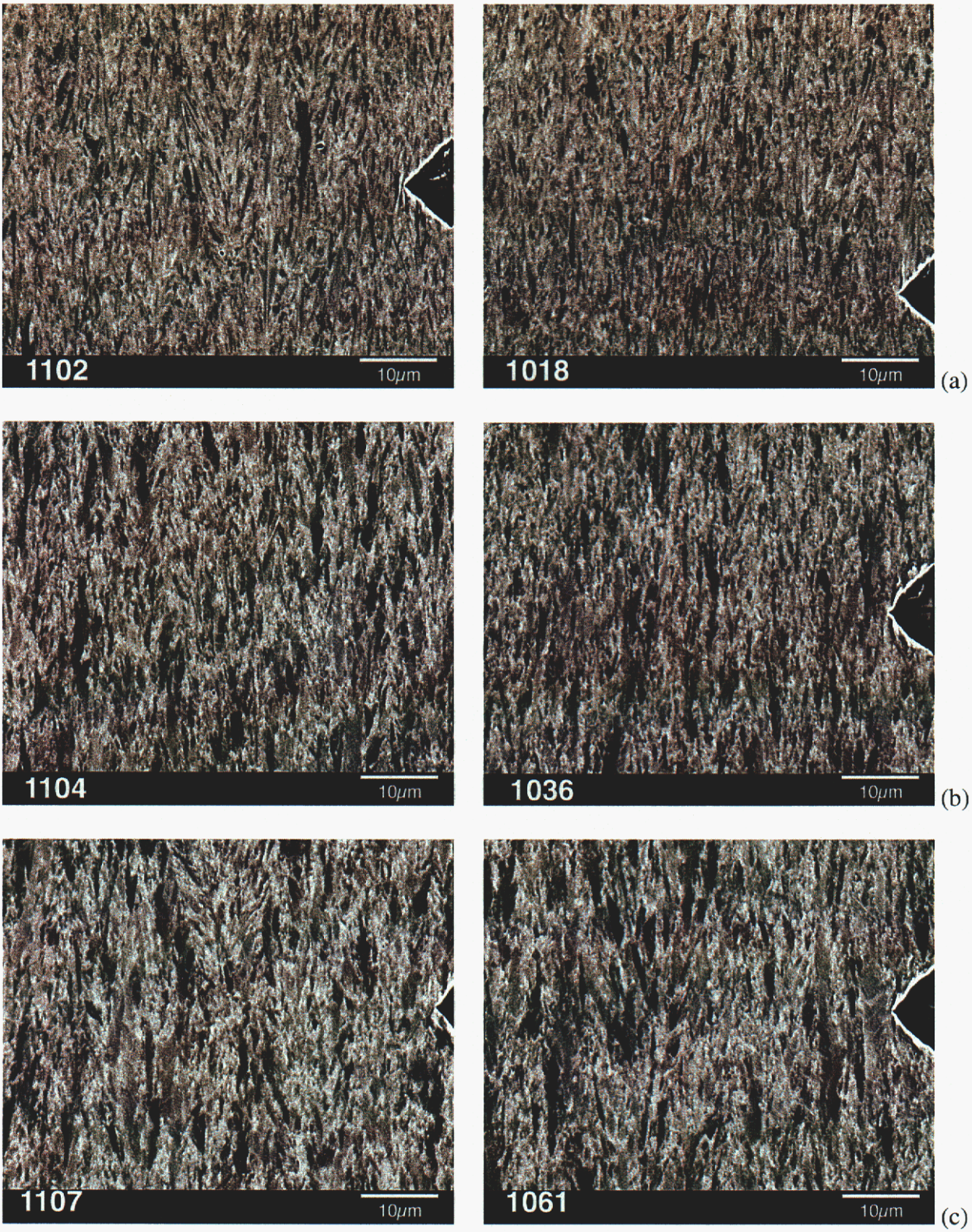


Figure 38. Grain structure before (on the left) and after (on the right) dormancy for material from (a) 13/31-307. (b) 13/36-351, and (c) 13/36-352.

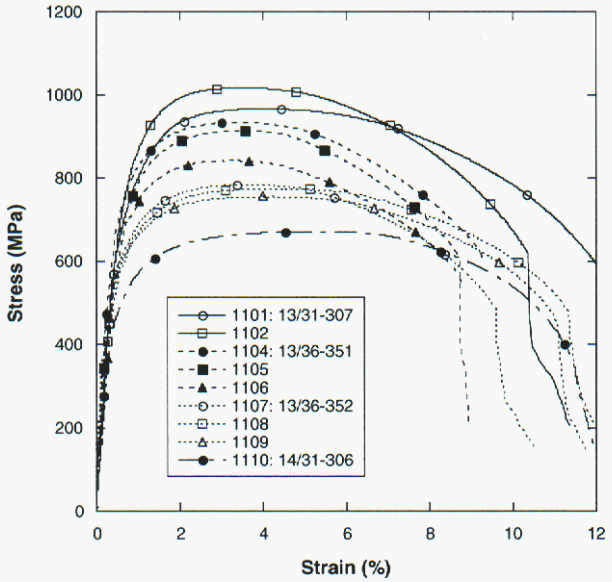


Figure 39. Stress-strain curves of as-plated tensile bars.

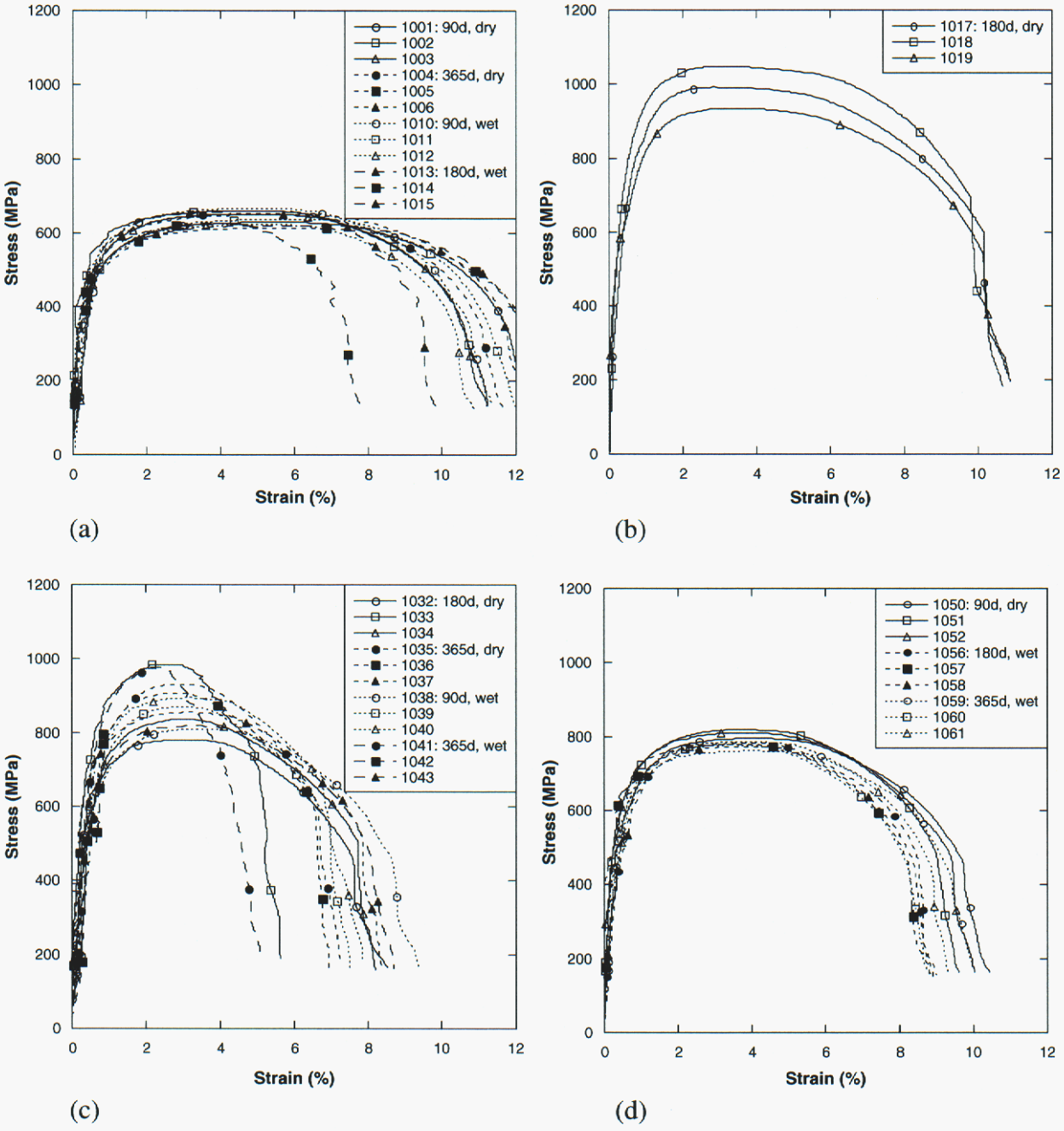


Figure 40. Stress-strain curves plotted by lot of material: (a) 14/31-306; (b) 13/31-307; (c) 13/36-351; and (d) 13/36-352.

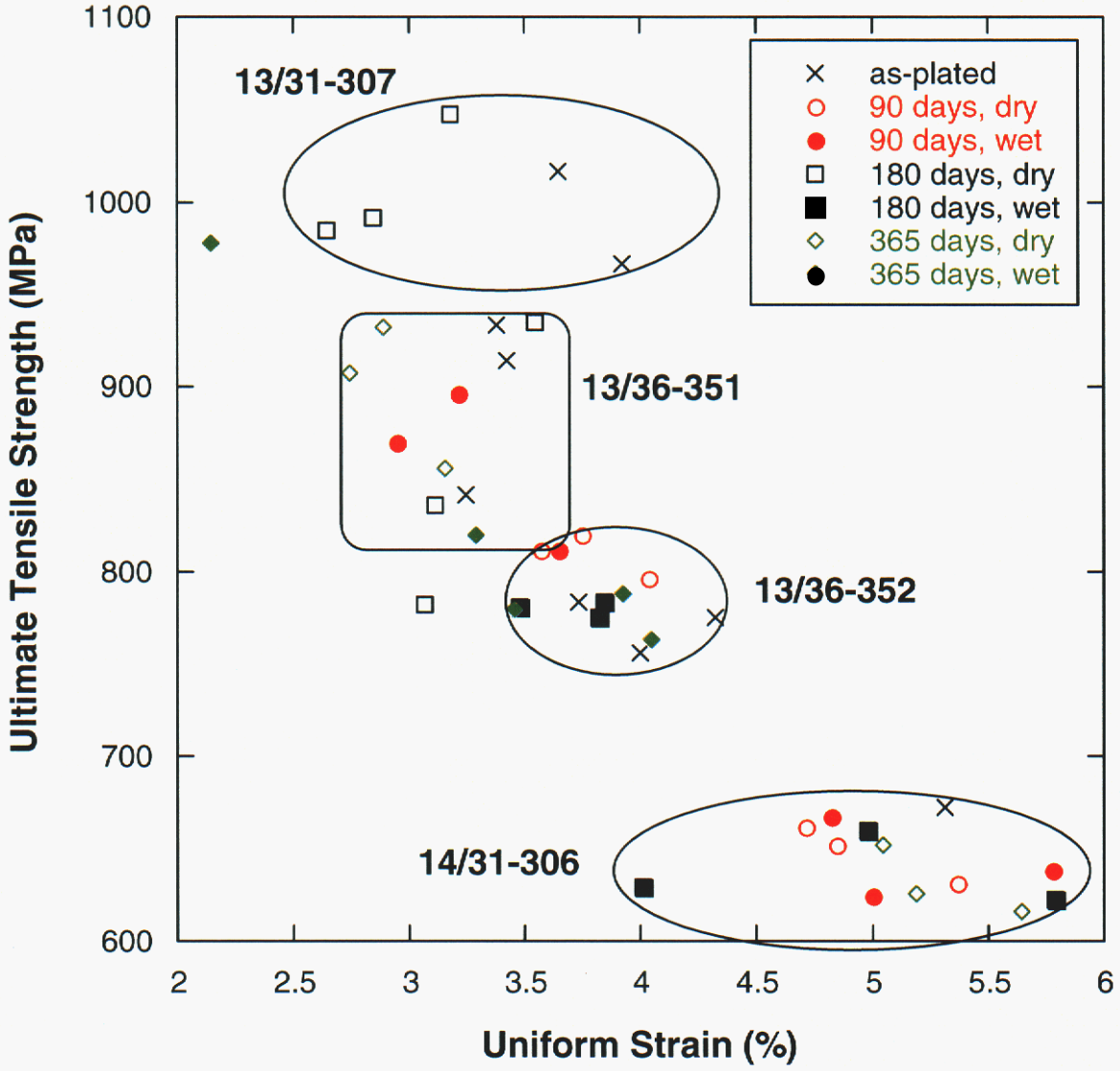


Figure 41. Ultimate tensile strength and uniform strain of dormancy tensile bars.

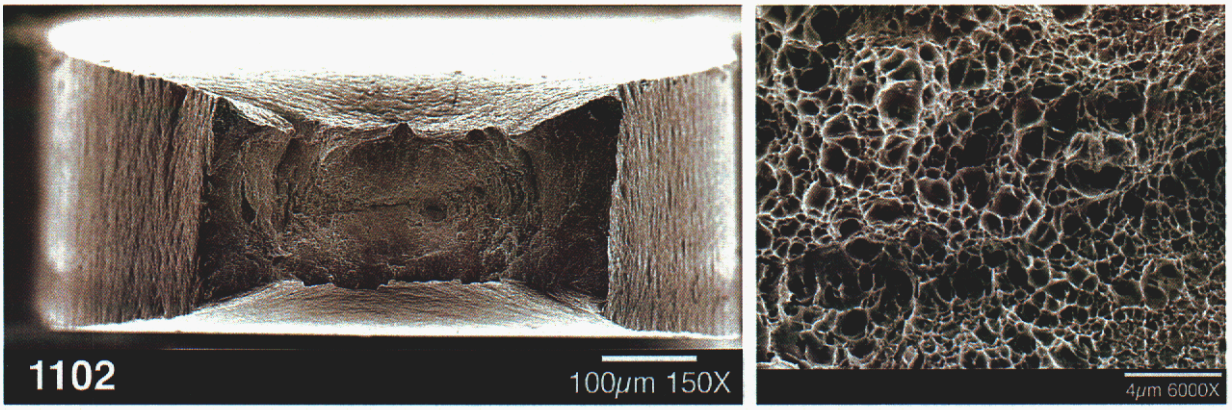


(a)

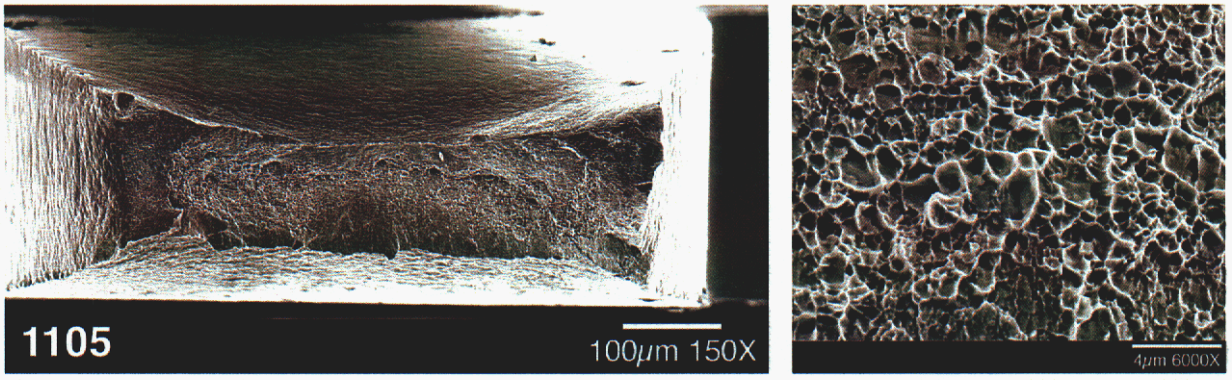


(b)

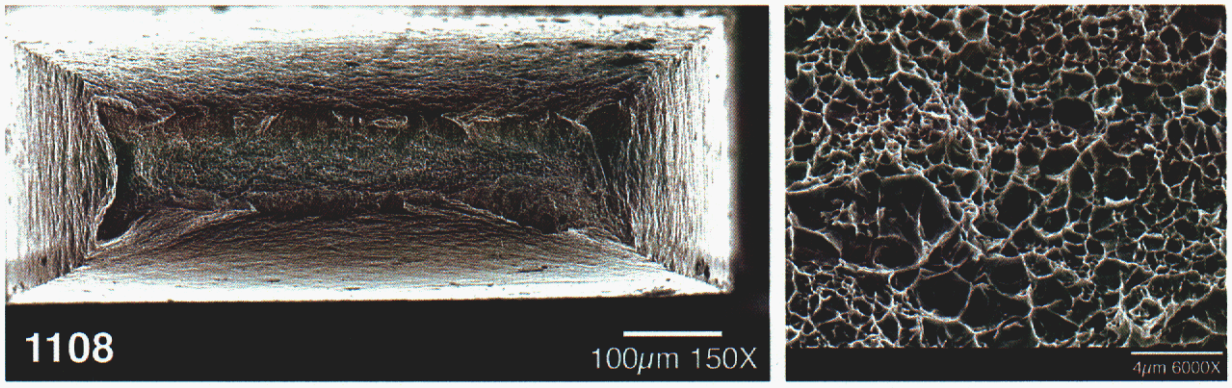


(c)

Figure 42. Fracture surfaces of as-plated specimens: (a) 13/31-307; (b) 13/36-351; and (c) 13/36-352.

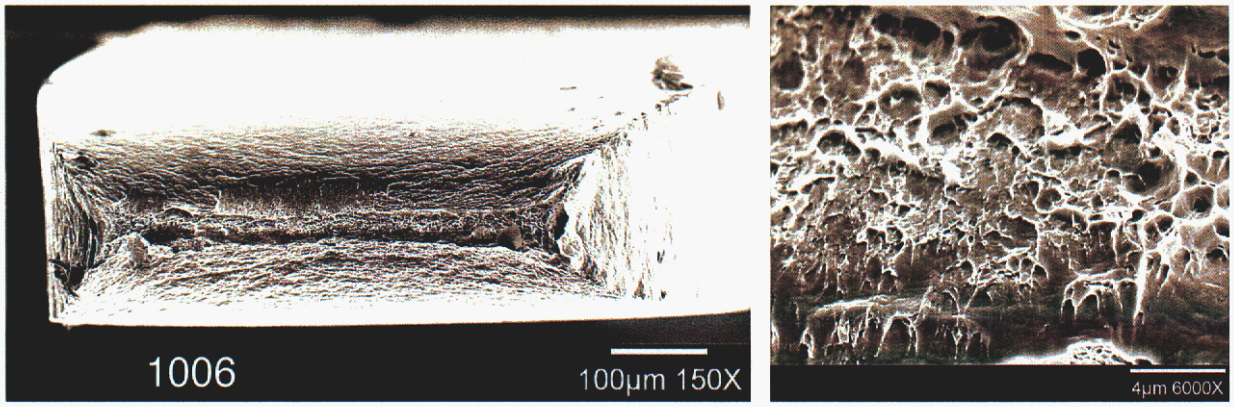


(a)

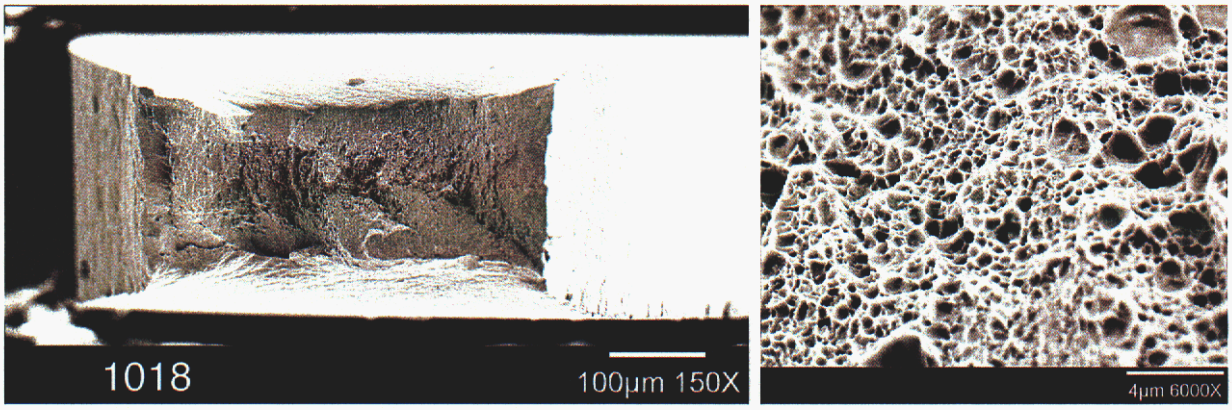


(b)

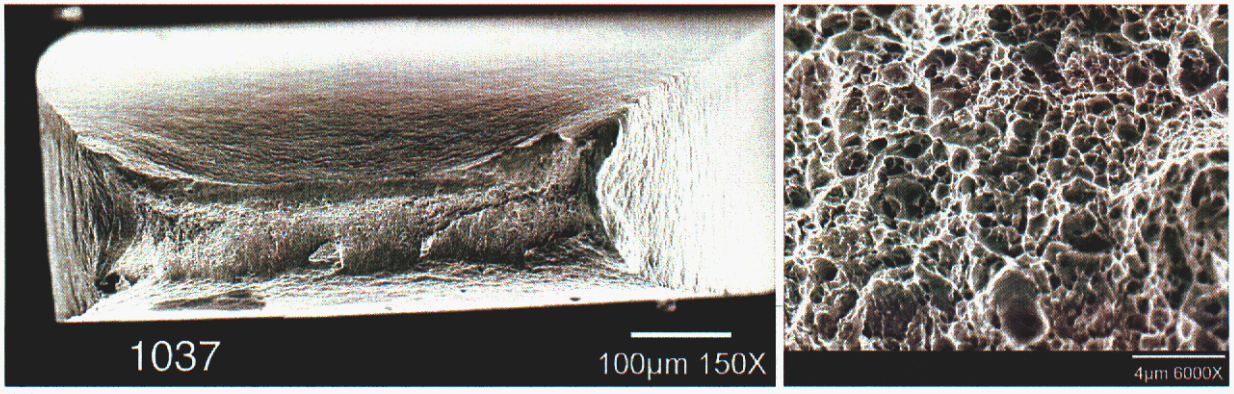


(c)

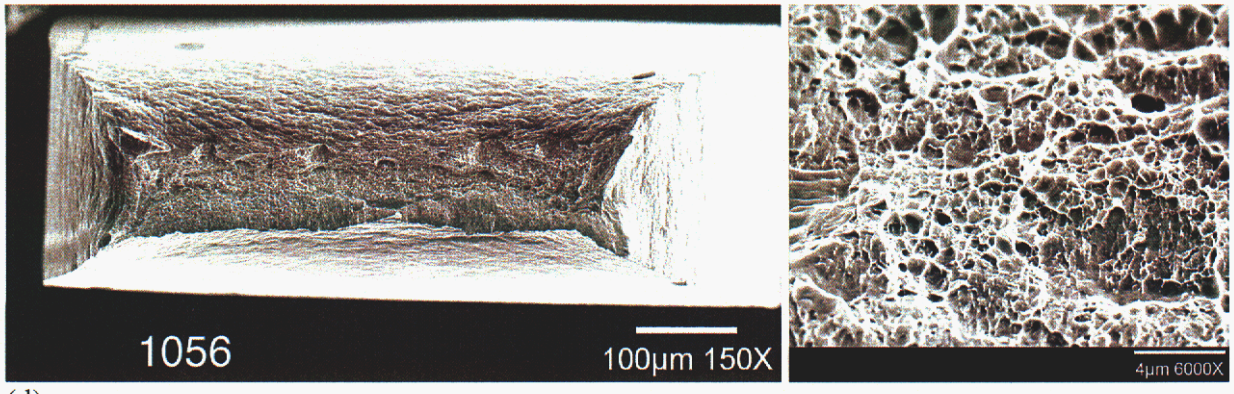


(d)

Figure 43. Fracture surfaces of specimens from four lots of material: (a) 14/31-306; (b); 13/31-307; (c) 13/36-351; and (d) 13/36-352.

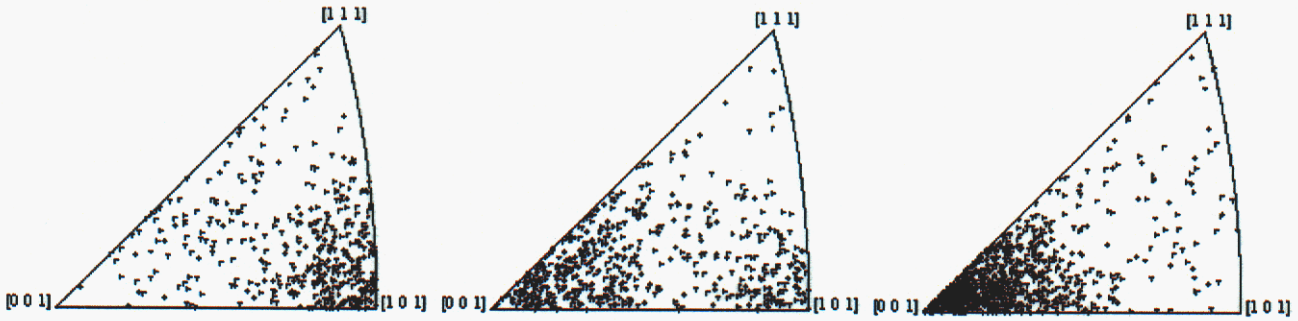


(a) (b) (c)

Figure 44. Pole figures generated by EBSD for material from lots (a) 13/31-307; (b) 13/36-351; and (c) 13/36-352 in the plating direction.

Table II. Part numbers and process identification of dormancy specimens.

| Part no. | Lot ID | Tank ID | Process Designation Tank / Lot |
|---|---|---|---|
| Tensile bars | | | |
| 1001-1016 | 31-306 | 14 | 14 / 31-306 |
| 1017-1031 | 31-307 | 13 | 13 / 31-307 |
| 1032-1049 | 36-351 | 13 | 13 / 36-351 |
| 1050-1068 | 36-352 | 13 | 13 / 36-352 |
| 1101-1102 | 31-307 | 13 | 13 / 31-307 |
| 1104-1106 | 36-351 | 13 | 13 / 36-351 |
| 1107-1109 | 36-352 | 13 | 13 / 36-352 |
| 1110 | 31-306 | 14 | 14 / 31-306 |
| Washers | | | |
| 2001-2016 | 30-291 | 14 | 14 / 30-291 |
| 2017-2032 | 30-300 | 13 | 13 / 30-300 |
| 2033-2039 | 30-291 | 14 | 14 / 30-291 |
| Gears | | | |
| 3001-3019 | 30-291 | 14 | 14 / 30-291 |
| 3020-3038 | 30-300 | 13 | 13 / 30-300 |
| 3039-3041 | 30-291 | 14 | 14 / 30-291 |
| U-springs | | | |
| 4001-4015 | 30-291 | 14 | 14 / 30-291 |
| 4016-4030 | 30-300 | 13 | 13 / 30-300 |
| 4031-4038 | 30-300 | 13 | 13 / 30-300 |
| 4039-4042 | 30-291 | 14 | 14 / 30-291 |

Table IIIa. Specimens and dormancy conditions

| Cylinder and conditions | Tensile bars | Washers | Gears | U-springs |
|---|---|---|---|---|
| | 1001 | 2003 | 3002 | 4002 |
| C1 | 1002 | 2004 | 3003 | 4003 |
| | 1003 | 2017 | 3020 | 4016 |
| 90 days | 1050 | 2018 | 3021 | 4017 |
| dry N2 | 1051 | | | |
| | 1052 | | | |
| | 1017 | 2005 | 3004 | 4004 |
| C2 | 1018 | 2006 | 3005 | 4005 |
| | 1019 | 2019 | 3022 | 4018 |
| 180 days | 1032 | 2020 | 3023 | 4019 |
| dry N2 | 1033 | | | |
| | 1034 | | | |
| | 1004 | 2007 | 3006 | 4006 |
| C3 | 1005 | 2008 | 3007 | 4007 |
| | 1006 | 2021 | 3024 | 4020 |
| 365 days | 1035 | 2022 | 3025 | 4021 |
| dryN2 | 1036 | | | |
| | 1037 | | | |
| | 1020 | 2009 | 3008 | 4008 |
| C4 | 1021 | 2010 | 3009 | 4009 |
| | 1022 | 2023 | 3026 | 4022 |
| 2 years | 1053 | 2024 | 3027 | 4023 |
| dry N2 | 1054 | | | |
| | 1055 | | | |

Table IIIb. Specimens and dormancy conditions

| Cylinder and conditions | Tensile bars | Washers | Gears | U-springs |
|---|---|---|---|---|
| | 1007 | 2011 | 3010 | 4010 |
| C5 | 1008 | 2012 | 3011 | 4011 |
| | 1009 | 2025 | 3028 | 4024 |
| 30 days | 1023 | 2026 | 3029 | 4025 |
| dry N2 | 1024 | | | |
| | 1025 | | | |

Table IIIc. Specimens and dormancy conditions

| Cylinder and conditions | Tensile bars | Washers | Gears | U-springs |
|---|---|---|---|---|
| | 1010 | 2013 | 3001 | 4012 |
| C6 | 1011 | 2014 | 3030 | 4031 |
| | 1012 | 2027 | 3012 | 4013 |
| 90 days | 1038 | 2028 | 3031 | 4032 |
| wet N2 | 1039 | | | |
| | 1040 | | | |
| | 1013 | 2015 | 3013 | 4014 |
| C7 | 1014 | 2016 | 3017 | 4015 |
| | 1015 | 2029 | 3032 | 4033 |
| 180 days | 1056 | 2030 | 3033 | 4034 |
| wet N2 | 1057 | | | |
| | 1058 | | | |
| | 1041 | 2033 | 3015 | 4035 |
| C8 | 1042 | 2034 | 3016 | 4036 |
| | 1043 | 2035 | 3039 | 4039 |
| 365 days | 1059 | 2036 | 3040 | 4040 |
| wet N2 | 1060 | | | |
| | 1061 | | | |
| | 1016 | 2032 | 3017 | 4037 |
| C9 | 1026 | 2037 | 3018 | 4038 |
| | 1027 | 2038 | 3019 | 4041 |
| 2 years | 1028 | 2039 | 3041 | 4042 |
| wet N2 | 1044 | | | |
| | 1045 | | | |

Table IV. Summary of the lots of material used for dormancy and the features that are characteristic of that material.

| Tank/lot | Specimens | General characteristics |
|---|---|---|
| 14/30-291 | Washers, gears, and u-springs | • porous lapped surfaces<br>• buttons on release (esp. u-springs) |
| 13/30-300 | Washers, gears, and u-springs | • buttons on release (esp. u-springs) |
| 14/31-306 | Tensile bars | • coarse grained<br>• lowest strength (~650MPa)<br>• smooth (some buttons) |
| 13/31-307 | Tensile bars | • highest strength (~1000MPa UTS)<br>• smooth (some buttons)<br>• scratches on lapped |
| 13/36-351 | Tensile bars | • fine grained (~900MPa UTS)<br>• river patterns on release<br>• scratches on lapped |
| 13/36-352 | Tensile bars | • largest grains and lowest strength (~800MPa UTS) from tank 13<br>• river patterns on release<br>• scratches on lapped |

Table Va. Tensile properties of as-plated material; 0.5% offset yield strength (0.5% sy), ultimate tensile strength (UTS), uniform elongation (eu), elongation at failure (ef).

| | Tensile bar ID | 0.5% sy (MPa) | UTS (MPa) | eu (%) | ef (%) |
|---|---|---|---|---|---|
| As-plated | 1101 | 774 | 967 | 3.92 | 12.06 |
| | 1102 | 846 | 1017 | 3.64 | 10.38 |
| | 1104 | 811 | 934 | 3.38 | 9.37 |
| | 1105 | 759 | 914 | 3.42 | 8.72 |
| | 1106 | 714 | 842 | 3.25 | 8.80 |
| | 1107 | 657 | 784 | 3.73 | 9.59 |
| | 1108 | 644 | 775 | 4.32 | 11.35 |
| | 1109 | 636 | 755 | 4.00 | 11.05 |
| | 1110 | 536 | 672 | 5.31 | 12.04 |

Table Vb. Tensile properties of dormancy specimens in dry N2; 0.5% offset yield strength (0.5% sy), ultimate tensile strength (UTS), uniform elongation (eu), elongation at failure (ef).

| Cylinder and conditions | Tensile bar ID | 0.5% sy (MPa) | UTS (MPa) | eu (%) | ef (%) |
|---|---|---|---|---|---|
| C1 90 days dry N2 | 1001 | 501 | 630 | 5.37 | 12.37 |
| | 1002 | 572 | 652 | 4.85 | 11.25 |
| | 1003 | 528 | 661 | 4.71 | 11.21 |
| | 1050 | 653 | 796 | 4.03 | 10.45 |
| | 1051 | 701 | 819 | 3.75 | 9.62 |
| | 1052 | 711 | 812 | 3.57 | 10.04 |
| C2 180 days dry N2 | 1017 | 844 | 992 | 2.85 | 10.86 |
| | 1018 | 942 | 1048 | 3.18 | 10.85 |
| | 1019 | 799 | 935 | 3.55 | 10.66 |
| | 1032 | 686 | 781 | 3.07 | 8.2 |
| | 1033 | 888 | 985 | -- | -- |
| | 1034 | 709 | 837 | 3.11 | 8.54 |
| C3 365 days dry N2 | 1004 | 538 | 653 | 5.19 | 11.64 |
| | 1005 | 489 | 615 | 5.65 | 12.95 |
| | 1006 | 514 | 651 | 5.04 | 12.38 |
| | 1035 | 777 | 931 | 2.89 | 7.23 |
| | 1036 | 777 | 907 | 2.74 | 6.93 |
| | 1037 | 763 | 856 | 3.16 | 8.38 |

C4: 2 years, dry N2; in dormancy through July 2004

Table Vc. Tensile properties of dormancy specimens in wet N2; 0.5% offset yield strength (0.5% sy), ultimate tensile strength (UTS), uniform elongation (eu), elongation at failure (ef).

| Cylinder and conditions | Tensile bar ID | 0.5% sy (MPa) | UTS (MPa) | eu (%) | ef (%) |
|---|---|---|---|---|---|
| | 1010 | 559 | 667 | 4.82 | 11.33 |
| C6 | 1011 | 498 | 638 | 5.78 | 11.99 |
| | 1012 | 505 | 624 | 5.00 | 10.86 |
| 90 days | 1038 | 667 | 812 | 3.65 | 9.42 |
| wet N2 | 1039 | 718 | 870 | 2.94 | 7.51 |
| | 1040 | 771 | 895 | 3.21 | 7.86 |
| | 1013 | 549 | 660 | -- | -- |
| C7 | 1014 | 530 | 629 | -- | -- |
| | 1015 | 503 | 622 | 5.79 | 12.48 |
| 180 days | 1056 | 612 | 784 | 3.85 | 8.91 |
| wet N2 | 1057 | 605 | 780 | 3.48 | 8.83 |
| | 1058 | 636 | 775 | 3.82 | 8.91 |
| | 1041 | 849 | 978 | -- | -- |
| C8 | 1042 | 804 | 804 | -- | -- |
| | 1043 | 690 | 819 | 3.29 | 8.72 |
| 365 days | 1059 | 653 | 762 | 4.05 | 10.08 |
| wet N2 | 1060 | 667 | 779 | 3.46 | 8.84 |
| | 1061 | 648 | 787 | 3.92 | 9.31 |
| C9: 2 years, wet N2; in dormancy through July 2004 | | | | | |

Table VI. Summary of the properties of the tensile bars before and after dormancy.

| Sample ID | | Microstructure | | | Hardness (VHN)* | Ultimate Tensile Strength (MPa)† |
|---|---|---|---|---|---|---|
| | | Surface morphology | | Grain structure | | |
| | | Release | Lapped | | | |
| 13/31-307 | Before | Smooth, some "buttons" | Scratches | Columnar Max width <1.5μm | 327 | 992±70 |
| | After | No change | | No change | 320 | 992±114 |
| 13/36-351 | Before | River patterns | Scratches and stains | Columnar Max width <2μm | 344 | 897±96 |
| | After | No change | | No change | 335 | 873±134 |
| 13/36-352 | Before | River patterns | Significant scratches | Columnar Max width 2-3μm | 285 | 771±30 |
| | After | No change | | No change | 289 | 788±36 |
| 14/31-306 | Before | Smooth, some "buttons" | Smooth | --- | --- | 672‡ |
| | After | No change | | Columnar Max width 4-5μm | 254 | 642±36 |

* average of five indentations spanning thickness from lapped to release sides.
† average values of three to twelve tests; uncertainty quoted as twice the standard deviation.
‡ single specimen

## Distribution List

| | | |
|---|---|---|
| 1 | MS 0323 | Chavez, D. - LDRD Office, 1011 |
| 1 | MS 0886 | Rye, Michael – 01822 |
| 1 | MS 0887 | Cieslak, M.J. – 01800 |
| 1 | MS 0889 | Buchheit, T.E. – 01851 |
| 1 | MS 0889 | Custer, J.S. – 01851 |
| 1 | MS 1411 | Hoyt, J.J. - 01851 |
| 1 | MS 1411 | Headley, T.J. - 01822 |
| 1 | MS 9001 | John, M.E. – 8000 |
| | | Attn: Stulen, R.H. – 8100, MS 9004 |
| | | Henson, D.R. - 8200, MS 9007 |
| | | McLean, W.J. - 8300, MS 9054 |
| | | Smith, P.N. - 8500, MS 9002 |
| | | Washington, K.E. - 8900, MS 9003 |
| 1 | MS 9036 | Cardinale, G.F. - 08245 |
| 1 | MS 9401 | Kelly, J.J. – 08753 |
| 1 | MS 9404 | Goods, S.H. - 08754 |
| 5 | MS 9402 | Cadden, C.H. – 08772 |
| 1 | MS 9402 | Chames, J.M. – 08773 |
| 1 | MS 9402 | Gardea, A.D. – 08773 |
| 1 | MS 9402 | Lucadamo, G.A. – 08773 |
| 1 | MS 9402 | San Marchi, C – 08772 |
| 5 | MS 9402 | Yang, N – 08773 |
| 1 | MS 9402 | Yio, Ja Lee – 08773 |
| 1 | MS 9402 | Wilson, Ken - 08770 |
| | | Attn: Bill Replogle, 08771 |
| | | Jim Wang, 08773 |
| | | Paul Spence, 08774 |
| 3 | MS 9018 | Central Technical Files, 8945-1 |
| 1 | MS 0899 | Technical Library, 9616 |
| 1 | MS 9021 | Classification Office, 8511, for Technical Library MS 0899, 9616 |
| | | DOE/OSTI via URL |

This page intentionally left blank